Inorganic Chemistry
Article

Inorg. Chem. **2010**, *49*, 5625–5641 **5625**
DOI: 10.1021/ic100521t

Role of Substitution on the Photophysical Properties of 5,5′-Diaryl-2,2′-bipyridine (bpy*) in $[Ir(ppy)_2(bpy^*)]PF_6$ Complexes: A Combined Experimental and Theoretical Study

Sébastien Ladouceur, Daniel Fortin, and Eli Zysman-Colman*

Département de chimie, Université de Sherbrooke, 2500 Boul. Université, Sherbooke, Quebec, Canada J1K 2R1

Received March 18, 2010

The synthesis of a family of 4′-functionalized 5,5′-diaryl-2,2′-bipyridines (bpy*; **6a**−**6g**) is reported. These ligands were reacted with the dimer $[(ppy)_2IrCl]_2$ (ppyH = 2-phenylpyridine) and afforded, after subsequent counterion exchange, a new series of luminescent cationic heteroleptic iridium(III) complexes, $[(ppy)_2Ir(bpy^*)]PF_6$ (**8a**−**8g**). These complexes were characterized by electrochemical and spectroscopic methods. The crystal structures of two of these complexes (**8a** and **8g**) are reported. All of the complexes except for **8c** and **8f** exhibit intense and long-lived emission in both 2-MeTHF and ACN at 77 K and room temperature. The origin of this emission has been assigned by computational modeling to be an admixture of ligand-to-ligand charge-transfer [^{3}LLCT; $\pi(ppy) \rightarrow \pi^*(bpy^*)$] and metal-to-ligand charge-transfer [^{3}MLCT; $d\pi(Ir) \rightarrow \pi^*(bpy^*)$] excited states that are primarily composed of the former. The luminescent properties for **8a**−**8c** are dependent upon the functionalization at the 4′ position of the aryl substituents affixed to the diimine ligand, while those for **8d**−**8g** are essentially independent because of an electronic decoupling of the aryls and bpy due to the substitution of *o*,*o*-dimethyl groups on the aryls, causing a near 90° angle between the aryl and bipyridyl moieties. A combined density functional theory (DFT)/time-dependent DFT study was conducted in order to understand the origin of the transitions in the absorption and emission spectra and to predict accurately emission energies for these complexes.

Introduction

Since the turn of the millennium, there has been a near-exponential interest in the study of the photophysical properties[1] of iridium(III) complexes and their applications in diverse fields such as organic light-emitting diodes (OLEDs)[2] and light-emitting electrochemical cells (LEECs) for next-generation visual displays,[2,3] catalysts for photoinduced cleavage of water for hydrogen production,[3v,4] biolabeling[5] and chemosensors[6] for oxygen,[7] organic salts,[8] and ions such as H^+,[8] F^-,[8] Cl^-,[9] Ca^{2+},[10] Hg^{2+},[11] and Ag^+.[12] The increased interest results from the privileged photophysical and electrochemical properties of iridium(III) complexes resulting from both the large ligand-field stabilization of iridium (color tuning) and the efficient intersystem crossing (high phosphorescent quantum yields) between the singlet and triplet excited states that is made possible by the high degree of spin−orbit coupling (ζ_{Ir} = 3909 cm^{-1}).[13] This, coupled with the use of strong-field cyclometallating ligands (C^N) such as phenylpyridine (ppyH), results in long-lived and highly luminescent[14] complexes that usually emit from metal-to-ligand charge transfer (^{3}MLCT), ligand-centered (^{3}LC), or mixed ^{3}MLCT/^{3}LC states,[14b,15] while rendering the thermal population of nonemissive metal-centered ^{3}MC states all but impossible, unlike $Ru(N^N)_3$ complexes [N^N = dimine such as bipyridine (bpy)].[16]

Heteroleptic iridium complexes of the form $[(C^N)_2Ir(N^N)]^+$ are of particular interest because of their facile capacity to finely modulate the emission energy through independent modification of the cyclometallating and ancillary ligands. Selective chemical substitution about the C^N ligands modulates the ^{3}LC state, while that of the N^N ligand controls the mixed ^{3}MLCT/^{3}LC state.[3g,j,x,15a,b,17] More specifically, placement of electron-donating groups on the ancillary ligand leads to an overall destabilization of the lowest unoccupied molecular orbital (LUMO) and a resulting blue shift in the emission spectrum.[18] Furthermore, these complexes possess reversible electrochemistry, are thermally stable, and can be easily accessed in two steps from $IrCl_3$.[3b,19] One particular disadvantage to charged heteroleptic complexes compared to their neutral homoleptic congeners of the form $Ir(C^N)_3$ is their relatively low quantum yields.

*To whom correspondence should be addressed. E-mail: Eli.Zysman-Colman@usherbrooke.ca.

(1) (a) Dixon, I. M.; Collin, J.-P.; Sauvage, J.-P.; Flamigni, L.; Susana, E.; Barigelletti, F. *Chem. Soc. Rev.* **2000**, *29*, 385. (b) Flamigni, L.; Barbieri, A.; Sabatini, C.; Ventura, B.; Barigelletti, F. *Top. Curr. Chem.* **2007**, *281*, 143. (c) Ulbricht, C.; Beyer, B.; Friebe, C.; Winter, A.; Schubert, U. S. *Adv. Mater.* **2009**, *21*, 4418.

(2) For a review of the science of OLEDs, see:Hung, L. S.; Chen, C. H. *Mater. Sci. Eng. Rep.* **2002**, *39*, 143.

Published on Web 05/25/2010

Whereas color tuning is reasonably well understood, it is far less clear what strategies to use to augment emission quantum yields. Recently, several examples[3c,d,i,l,18,20] of highly luminescent [min 20% and up to 85% in acetonitrile (ACN)] cationic heteroleptic complexes have been reported, but these, unsurprisingly, mostly emit at high energy in the green-to-blue region, adhering to the energy gap law that describes the dependence of nonradiative decay processes (and thus the quantum yield) on the emission energy of the luminophore.[21] A key challenge in LEEC design is to develop strategies that enable controlled color tuning, especially in the red, green, and blue regions, without adversely affecting phosphorescent quantum yields. Architectures that can meet this challenge would thus be highly desirable.

In this paper, we report the synthesis of a new family of 5,5′-diarylbipyridines (bpy*) and their incorporation as ancillary ligands into luminescent cationic iridium complexes of the general formula $[(ppy)_2Ir(bpy^*)]PF_6$. This family is subdivided into two series: the first series contains aryl groups substituted with electron-releasing groups at the 4′ position, while the second series also possesses methyl groups at the 2′ and 6′ positions. The latter series is designed to sequester the arenes into an orthogonal orientation relative to the diimine. The two series of isostructural complexes systematically probe the interplay between the conjugative effects and electron-releasing power of remote substituents, while simultaneously protecting the iridium center due to their steric effects. These are compared to an archetypal complex, $[(ppy)_2Ir(bpy)]^+$. A detailed photophysical and electrochemical investigation is described in order to assess the aforementioned structure−property relationship and its impact on the quantum efficiency. We will show that the majority of these complexes emit from an admixture of ligand-to-ligand charge-transfer (^{3}LLCT)/^{3}MLCT states, while complexes possessing potent electron-releasing substituents on the aryls emit from an intraligand charge-transfer (^{3}ILCT) state with a marked decrease in the quantum yields.

A combined density functional theory (DFT) and time-dependent DFT (TD-DFT) study provides insight into the nature of the ground (S_0) and excited (S_1 and T_1) states with resulting detailed assignments of the orbitals involved in absorption and emission transitions. The theoretical analysis corroborates the experimental study. These will serve to guide ligand design to develop complexes for better performing OLEDs for visual display and lighting applications.

(3) (a) Baldo, M. A.; Thompson, M. E.; Forrest, S. R. *Nature* **2000**, *403*, 750. (b) Baldo, M. A.; Lamansky, S.; Burrows, P. E.; Thompson, M. E.; Forrest, S. R. *Appl. Phys. Lett.* **1999**, *75*, 4. (c) Nazeeruddin, M. K.; Wegh, R. T.; Zhou, Z.; Klein, C.; Wang, Q.; DeAngelis, F.; Fantacci, S.; Grätzel, M. *Inorg. Chem.* **2006**, *45*, 9245. (d) Bolink, H. J.; Cappelli, L.; Coronado, E.; Gratzel, M.; Orti, E.; Costa, R. D.; Viruela, P. M.; Nazeeruddin, M. K. *J. Am. Chem. Soc.* **2006**, *128*, 14786. (e) Slinker, J. D.; Gorodetsky, A. A.; Lowry, M. S.; Wang, J.; Parker, S. T.; Rohl, R.; Bernhard, S.; Malliaras, G. G. *J. Am. Chem. Soc.* **2004**, *126*, 2763. (f) Slinker, J. D.; Bernards, D. A.; Houston, P. L.; Abruña, H. D.; Bernhard, S.; Malliaras, G. G. *Chem. Commun.* **2003**, *19*, 2392. (g) Lowry, M. S.; Hudson, W. R.; Pascal, R. A., Jr.; Bernhard, S. *J. Am. Chem. Soc.* **2004**, *126*, 14129. (h) Slinker, J. D.; Koh, C. Y.; Malliaras, G. G.; Lowry, M. S.; Bernhard, S. *Appl. Phys. Lett.* **2005**, *86*, 173506. (i) Tamayo, A. B.; Garon, S.; Sajoto, T.; Djurovich, P. I.; Tsyba, I. M.; Bau, R.; Thompson, M. E. *Inorg. Chem.* **2005**, *44*, 8723. (j) Lowry, M. S.; Bernhard, S. *Chem.—Eur. J.* **2006**, *12*, 7970. (k) Su, H.-C.; Wua, C.-C.; Fang, F.-C.; Wong, K.-T. *Appl. Phys. Lett.* **2006**, *89*, 261118. (l) Su, H.-C.; Fang, F.-C.; Hwu, T.-Y.; Hsieh, H.-H.; Chen, H.-F.; Lee, G.-H.; Peng, S.-M.; Wong, K.-T.; Wu, C.-C. *Adv. Funct. Mater.* **2007**, *17*, 1019. (m) Slinker, J. D.; Rivnay, J.; Moskowitz, J. S.; Parker, J. B.; Bernhard, S.; Abruña, H. D.; Malliaras, G. G. *J. Mater. Chem.* **2007**, *17*, 2976. (n) Neve, F.; LaDeda, M.; Crispini, A.; Bellusci, A.; Puntoriero, F.; Campagna, S. *Organometallics* **2004**, *23*, 5856. (o) Lee, J. K.; Yoo, D. S.; Handy, E. S.; Rubner, M. F. *Appl. Phys. Lett.* **1996**, *69*, 1686. (p) Maness, K. M.; Masui, H.; Wightman, R. M.; Murray, R. W. *J. Am. Chem. Soc.* **1997**, *119*, 3987. (q) Handy, E. S.; Pal, A. J.; Rubner, M. F. *J. Am. Chem. Soc.* **1999**, *121*, 3525. (r) Gao, F. G.; Bard, A. J. *J. Am. Chem. Soc.* **2000**, *122*, 7426. (s) Buda, M.; Kalyuzhny, G.; Bard, A. J. *J. Am. Chem. Soc.* **2002**, *124*, 6090. (t) Bernhard, S.; Barron, J. A.; Houston, P. L.; Abruña, H. D.; Ruglovsky, J. L.; Gao, X.; Malliaras, G. G. *J. Am. Chem. Soc.* **2002**, *124*, 13624. (u) Rudmann, H.; Shimada, S.; Rubner, M. F. *J. Appl. Phys.* **2003**, *94*, 115. (v) Lowry, M. S.; Goldsmith, J. I.; Slinker, J. D.; Rohl, R.; Pascal, R. A.; Malliaras, G. G.; Bernhard, S. *Chem. Mater.* **2005**, *17*, 5712. (w) Rudmann, H.; Shimida, S.; Rubner, M. F. *J. Am. Chem. Soc.* **2002**, *124*, 4918. (x) Nazeeruddin, M. K.; Hunmphry-Baker, R.; Berner, D.; Rivier, B. S.; Zuppiroli, L.; Grätzel, M. *J. Am. Chem. Soc.* **2003**, *125*, 8790. (y) Zysman-Colman, E.; Slinker, J. D.; Parker, J. B.; Malliaras, G. G.; Bernhard, S. *Chem. Mater.* **2008**, *20*, 388. (z) Adachi, C.; Baldo, M. A.; Thompson, M. E.; Forrest, S. R. *Appl. Phys.* **2001**, *90*, 5048. (aa) Bolink, H. J.; Coronado, E.; Costa, R. D.; Ort, E.; Sessolo, M.; Graber, S.; Doyle, K.; Neuburger, M.; Housecroft, C. E.; Constable, E. C. *Adv. Mater.* **2008**, *20*, 3910.

(4) (a) Tinker, L. L.; McDaniel, N. D.; Curtin, P. N.; Smith, C. K.; Ireland, M. J.; Bernhard, S. *Chem.—Eur. J.* **2007**, *13*, 8726. (b) Goldsmith, J. I.; Hudson, W. R.; Lowry, M. S.; Anderson, T. H.; Bernhard, S. *J. Am. Chem. Soc.* **2005**, *127*, 7502.

(5) (a) Lo, K. K.-W.; Ng, D. C.-M.; Chung, C.-K. *Organometallics* **2001**, *20*, 4999. (b) Iridium complexes have been incorporated into dendritic structures. See: Lo, S. C.; Namdas, E. B.; Burn, P. L.; Samuel, I. D. W. *Macromolecules* **2003**, *36*, 9721. (c) Lo, K. K.-W.; Chung, C.-K.; Zhu, N. *Chem.—Eur. J.* **2003**, *9*, 475. (d) Lo, K. K.-W.; Chung, C.-K.; Lee, T. K.-M.; Lui, L.-H.; Tsang, K. H.-K.; Zhu, N. *Inorg. Chem.* **2003**, *42*, 6886. (e) Lo, K. K.-W.; Chan, J. S.-W.; Chung, C.-K.; Tsang, V. W.-H.; Zhu, N. *Inorg. Chim. Acta* **2004**, *357*, 3109. (f) Lo, K. K.-W.; Hui, W.-K.; Chung, C.-K.; Tsang, K. H.-K.; Ng, D. C.-M.; Zhu, N.; Cheung, K.-K. *Coord. Chem. Rev.* **2005**, *249*, 1434. (g) Lo, K. K.-W.; Lau, J. S.-Y. *Inorg. Chem.* **2007**, *46*, 700. (h) Lo, K. K.-W.; Zhang, K. Y.; Leung, S.-K.; Tang, M.-C. *Angew. Chem., Int. Ed.* **2008**, *47*, 2213. (i) Lo, K. K.-W.; Chan, J. S.-W.; Lui, L.-H.; Chung, C.-K. *Organometallics* **2004**, *23*, 3108.

(6) Kim, J. I.; Shin, I.-S.; Kim, H.; Lee, J.-K. *J. Am. Chem. Soc.* **2005**, *127*, 1614.

(7) Di Marco, G.; Lanza, M.; Mamo, A.; Stefio, I.; Di Pietro, C.; Romeo, G.; Campagna, S. *Anal. Chem.* **1998**, *70*, 5019.

(8) Zhao, Q.; Liu, S.; Shi, M.; Li, F.; Jing, H.; Yi, T.; Huang, C. *Organometallics* **2007**, *26*, 5922.

(9) Goodall, W.; Williams, J. A. G. *J. Chem. Soc., Dalton Trans.* **2000**, 2893.

(10) Ho, M.-L.; Hwang, F.-M.; Chen, P.-N.; Hu, Y.-H.; Cheng, Y.-M.; Chen, K.-S.; Lee, G.-H.; Chi, Y.; Chou, P.-T. *Org. Biomol. Chem.* **2006**, *4*, 98.

(11) Zhao, Q.; Cao, T.; Li, F.; Li, X.; Jing, H.; Yi, T.; Huang, C. *Organometallics* **2007**, *26*, 2077.

(12) Schmittel, M.; Lin, H. *Inorg. Chem.* **2007**, *46*, 9139.

(13) Montalti, M.; Credi, A.; Prodi, L.; Gandolfi, M. T. *Handbook of Photochemistry*; Taylor and Francis: Boca Raton, FL, 2006.

(14) (a) Ohsawa, Y.; Sprouse, S.; King, K. A.; DeArmond, M. K.; Hanck, K. W.; Watts, R. J. *J. Phys. Chem.* **1987**, *91*, 1047. (b) Garces, F. O.; King, K. A.; Watts, R. J. *Inorg. Chem.* **1988**, *27*, 3464.

(15) (a) Colombo, M. G.; Hauser, A.; Güdel, H. U. *Inorg. Chem.* **1993**, *32*, 3088. (b) Colombo, M. G.; Güdel, H. U. *Inorg. Chem.* **1993**, *32*, 3081. (c) Colombo, M. G.; Brunold, T. C.; Riedener, T.; Guedel, H. U.; Fortsch, M.; Buergi, H.-B. *Inorg. Chem.* **1994**, *33*, 545.

(16) Goze, C.; Chambron, J.-C.; Heitz, V.; Pomeranc, D.; Salom-Roig, X. J.; Sauvage, J.-P.; Morales, A. F.; Barigelletti, F. *Eur. J. Inorg. Chem.* **2003**, *2003*, 3752.

(17) (a) Avilov, I.; Minoofar, P.; Cornil, J.; De Cola, L. *J. Am. Chem. Soc.* **2007**, *129*, 8247. (b) Hay, P. J. *J. Phys. Chem. A* **2002**, *106*, 1634. (c) Lamansky, S.; Djurovich, P.; Murphy, D.; Abdel-Razzaq, F.; Kwong, R.; Tsyba, I.; Bortz, M.; Mui, B.; Bau, R.; Thompson, M. E. *Inorg. Chem.* **2001**, *40*, 1704. (d) Lamansky, S.; Djurovich, P.; Murphy, D.; Abdel-Razzaq, F.; Lee, H.-E.; Adachi, C.; Burrows, P. E.; Forrest, S. R.; Thompson, M. E. *J. Am. Chem. Soc.* **2001**, *123*, 4304. (e) Li, J.; Djurovich, P. I.; Alleyne, B. D.; Yousufuddin, M.; Ho, N. N.; Thomas, J. C.; Peters, J. C.; Bau, R.; Thompson, M. E. *Inorg. Chem.* **2005**, *44*, 1713. (f) Kwon, T.-H.; Cho, H. S.; Kim, M. K.; Kim, J.-W.; Kim, J.-J.; Lee, K. H.; Park, S. J.; Shin, I.-S.; Kim, H.; Shin, D. M.; Chung, Y. K.; Hong, J.-I. *Organometallics* **2005**, *24*, 1578.

(18) De Angelis, F.; Fantacci, S.; Evans, N.; Klein, C.; Zakeeruddin, S. M.; Moser, J.-E.; Kalyanasundaram, K.; Bolink, H. J.; Gratzel, M.; Nazeeruddin, M. K. *Inorg. Chem.* **2007**, *46*, 5989.

(19) King, K. A.; Watts, R. J. *J. Am. Chem. Soc.* **1987**, *109*, 1589.

(20) Lafolet, F.; Welter, S.; Popovic, Z.; Cola, L. D. *J. Mater. Chem.* **2005**, *15*, 2820.

(21) Caspar, J. V.; Kober, E. M.; Sullivan, B. P.; Meyer, T. J. *J. Am. Chem. Soc.* **1982**, *104*, 630.

Scheme 1[a]

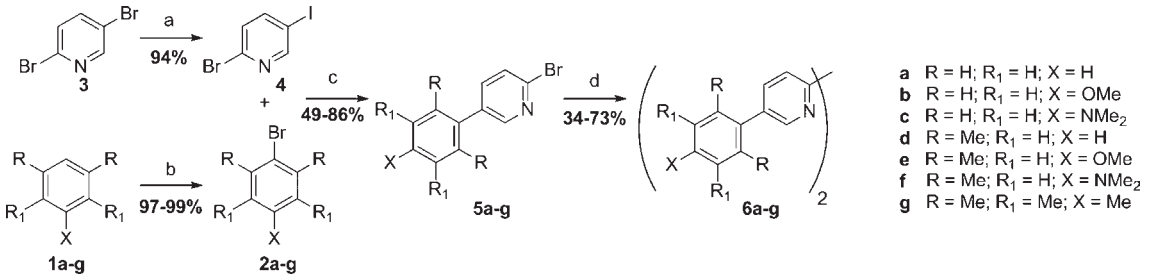

[a] (a) (i) 1.1 equiv of *n*-BuLi/Et_2O, −78 °C, 30 min; (ii) 1.1 equiv of I_2/Et_2O, −78 °C to RT, 16 h. (b) 1 equiv of NBS/ACN, 0 °C to RT, 16 h. (c) (i) 1.1 equiv of *n*-BuLi/THF, −78 °C, 30 min; (ii) 0.7 equiv of $ZnCl_2$/THF, −78 °C to RT, 30 min; (iii) 1 equiv of **4**, 1.6 mol % $Pd(PPh_3)_4$/THF, reflux, 18 h. (d) (i) 1.1 equiv of *n*-BuLi/THF, −78 °C, 30 min; (ii) 1.1 equiv of $ZnCl_2$/THF, −78 °C to RT, 30 min; (iii) 1 equiv of **5a**−**5g**, 5 mol % $Pd(PPh_3)_4$/THF, reflux, 18 h.

Results and Discussion

Synthesis. The targeted bpy* ligands were obtained from the corresponding arene via a three-step protocol (Scheme 1). Arenes **1b**, **1c**, and **1e**−**1g** were brominated regioselectively using *N*-bromosuccinimide (NBS) in ACN to afford **2b**, **2c**, and **2e**−**2g** in excellent yield, 97−99%; **2a** and **2d** were available commercially.[22] These bromoarenes were then subjected to a palladium-catalyzed Negishi[23] cross-coupling reaction with 2-bromo-5-iodopyridine (**4**), itself obtained in 94% via iodine quench of the lithiate formed by a metal−halogen exchange[24] of 2,5-dibromopyridine (**3**). 2-Bromo-5-arylpyridines **5a**−**5g** were then homocoupled under Negishi conditions to afford bpy* **6a**−**6g** with overall yields ranging from 34 to 73% over the three-step linear sequence (Table 1) under nonoptimized conditions. Nevertheless, the iterative Negishi protocol proved to be an acceptable, straightforward, and general method for accessing functionalized bpy*. Bipyridines **6a** and **6d**−**6g** were all found to be readily soluble in a plethora of organic solvents; however, **6b** and **6c** were poorly soluble, most probably because of increased conjugation.[23b]

With **6a**−**6g** obtained, scission of the μ-dichloro-bridged iridium dimer[25] **7** occurred readily to afford heteroleptic $[(ppy)_2Ir(bpy^*)]^+$ complexes (**8a**−**8g**) in good-to-excellent yield. These complexes were isolated as their PF_6^- salts after anion metathesis of the chloride (Scheme 2). The archetypal $[(ppy)_2Ir(bpy)]PF_6$ (**9**) was also synthesized to serve as an external standard and reference complex. All complexes were recrystallized (cf. the Supporting Information, SI). Characterization of ligands and complexes by melting point (mp) determination, ^1H NMR and ^{13}C NMR spectroscopy, and low- and high-resolution mass spectrometry provided satisfactory microanalysis.

Solid-State Structures from X-ray Crystallography. X-ray-quality single-crystal structures, depicted in Figure 1, for two (**8a** and **8g**) of the seven complexes were obtained by slow vapor diffusion of *tert*-butyl methyl ether into a chlorobenzene solution. Complex **8a** crystallizes in an orthorhombic *Pbca* space group, while **8g** crystallizes in a triclinic $P\bar{1}$ space group. The average Ir−C_{ppy}, Ir−N_{ppy}, and Ir−N_{bpy} bond lengths are unremarkable when compared with other $[(ppy)_2Ir(bpy)]^+$-type complexes (1.994 ± 0.012, 2.047 ± 0.009, and 2.134 ± 0.017 Å, respectively, for **8a**; 2.037 ± 0.013, 2.011 ± 0.023, and 2.148 ± 0.010 Å, respectively, for **8g**).[3n,5c,e,26] The longer Ir−N_{bpy} bond is

Table 1. Synthesis of **6a**−**6g**

Entry	Aryls		Yield of **2a-g** (%)	Yield of **5a-g** (%)	Yield of **6a-g** (%)
1		**a**	-	72	43
2	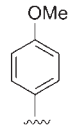	**b**	98	86	52
3	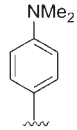	**c**	97	67	70
4	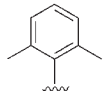	**d**	-	68	34
5	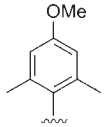	**e**	99	55	67
6	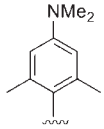	**f**	99	49	73
7	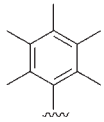	**g**	99	54	39

(22) Zysman-Colman, E.; Arias, K.; Siegel, J. S. *Can. J. Chem.* **2009**, *87*, 440.
(23) (a) Negishi, E. *Handbook of Organopalladium Chemistry for Organic Synthesis*; Wiley: New York, 2002. (b) Loren, J. C.; Siegel, J. S. *Angew. Chem., Int. Ed.* **2001**, *40*, 754.
(24) (a) Parham, W. E.; Piccirilli, R. M. *J. Org. Chem.* **1977**, *42*, 257. (b) Wang, X.; Rabbat, P.; O'Shea, P.; Tillyer, R.; Grabowski, E. J. J.; Reider, P. J. *Tetrahedron Lett.* **2000**, *41*, 4335.
(25) Nonoyama, M. *Bull. Chem. Soc. Jpn.* **1974**, *47*, 767.
(26) (a) Neve, F.; Crispini, A.; Campagna, S.; Serroni, S. *Inorg. Chem.* **1999**, *38*, 2250. (b) Cheung, K.-M.; Zhang, Q.-F.; Chan, K.-W.; Lam, M. H. W.; Williams, I. D.; Leung, W.-H. *J. Organomet. Chem.* **2005**, *690*, 2913. (c) Neve, F.; Crispini, A. *Eur. J. Inorg. Chem.* **2000**, *2000*, 1039. (d) Lepeltier, M.; Lee, T. K.-M.; Lo, K. K.-W.; Toupet, L.; Le Bozec, H.; Guerchais, V. *Eur. J. Inorg. Chem.* **2005**, *2005*, 110. (e) Urban, R.; Krämer, R.; Mihan, S.; Polborn, K.; Wagner, B.; Beck, W. *J. Organomet. Chem.* **1996**, *517*, 191.

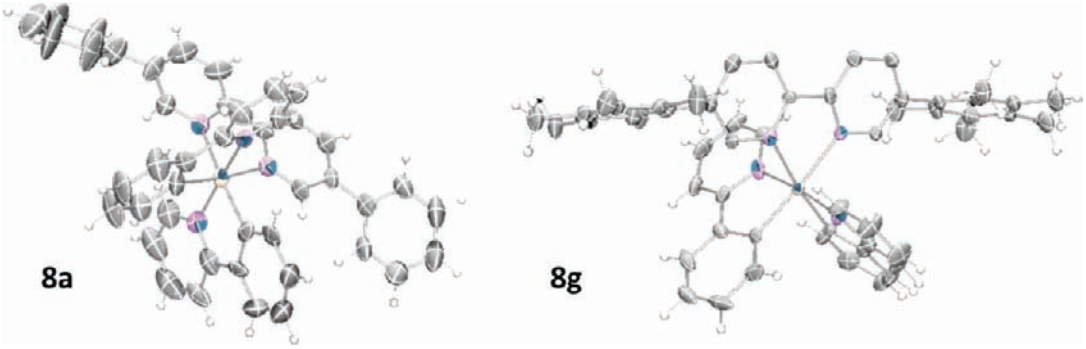

Figure 1. ORTEP perspective representations of complexes **8a** and **8g** (ellipsoids at 50% probability). The counterion PF_6^- has been removed for clarity.

Scheme 2[a]

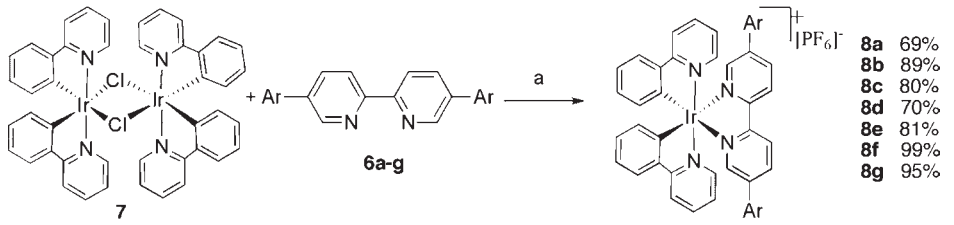

[a] (a) (i) ethylene glycol, 150 °C, 18 h; (ii) NH_4PF_6(aq).

due to the large trans influence imparted by the cyclometalated carbon of the ppy ligands; the ppy ligands are oriented in a mutually cis configuration, which is the same as that in dimer **7**.[1b] The overall geometry for each is that of a distorted octahedron with $(C-Ir-N)_{avg}$ and N−Ir−N bite angles of 80.5 ± 0.3° and 89.9 ± 0.1° for **8a** and 79.7 ± 0.1° and 76.8 ± 0.1° for **8g**. The latter complex is slightly more distorted in order to accommodate the bulkier pentamethylphenyl groups attached to the bpy fragment.

The primary difference in structure between the two complexes resides in the dihedral angles measured between the plane of the arene and that of the bpy. For **8a**, the average dihedral angle is 36 ± 3°, while for **8g**, it is 60 ± 5°; the unexpectedly low dihedral angle for **8g** is most likely due to crystal-packing forces. Indeed, the computed ground-state geometry for **8g** predicts a dihedral angle of ca. 90° (vide infra). The pseudo-orthogonal disposition in **8g** with respect to the mean plane of the bpy is primarily due to the presence of the *o*,*o*-dimethyl groups. The methyl groups act to impede conjugation and to limit rotation about the aryl−pyridyl bond. This elevated barrier to rotation is also evident spectroscopically, and its determination will be discussed below.

NMR Analysis of Solution Conformation. ^1H and ^{13}C NMR spectra were obtained for all ligands and complexes. The ^1H NMR spectra for the latter are shown in Figure 2. For **8a**−**8g**, each of the aromatic protons was resolved by ^1H NMR. We noted a large upfield shift of several of these signals upon metathesis of the chloride salt to the hexafluorophosphate salt, notably the α-proton designated H_6(bpy) (e.g., for **8b**, see Figure S1 in the SI). Thus, the counterion influences strongly the local electronic environment around the iridium center, with the bulkier PF_6^- being more loosely associated with the iridium complex than the chloride. Such an influence does not necessarily translate into perturbations in the photophysical properties (absorption and emission). Bernhard and co-workers had previously demonstrated that the chloride and hexafluorophosphate salts of a large family of heteroleptic iridium complexes exhibited nearly identical emission maxima.[3g]

The ^1H NMR spectra of **8a**−**8c** recorded in $CDCl_3$ at room temperature (RT) exhibit the expected C_2 symmetry (Figure 2).[19,27] As the aryl substituent becomes more electron-rich, the α-proton signal on the bpy is shifted upfield from 9 to 8.5 ppm. The ^1H NMR spectra of **8d**−**8f** recorded in $CDCl_3$ at RT exhibit the same trend, but it is attenuated relative to that observed for **8a**−**8c** because of the loss of conjugation. Of particular interest is the apparition of nonequivalent methyl peaks in the aliphatic region in each of **8d**−**8g**. For instance, all five methyl groups about the aryl fragment are diastereotopic for **8g**. The presence of only five signals is indicative of a localized σ_v mirror plane that renders the two aryls attached to the bpy ligand enantiomorphic. The particular features of this spectrum can be explained in terms of a ground-state geometry that situates the arene perpendicular to the bpy plane in concert with an elevated rotational barrier about the $C_{aryl}-C_{bpy}$ bond. A similar set of observations were made for each of **8d**−**8f**. Here, two singlets were observed in the aliphatic region, integrating with a ratio of 1:1. Diastereotopic aryl protons were also clearly differentiated for **8e**, while those for **8f** were unresolved but their signals were broadened. Rotational barriers for **8a**, **8d**, and **8g** were calculated, and these results will be discussed below.

Solution-State Photophysical Properties. Absorption. The photophysical properties of **8a**−**8g** were investigated and compared to those of $[(ppy)_2Ir(bpy)]PF_6$ (**9**). The absorption spectra are shown in Figure 3 and the data

(27) Garces, F. O.; Watts, R. J. *Magn. Reson. Chem.* **1993**, *31*, 529.

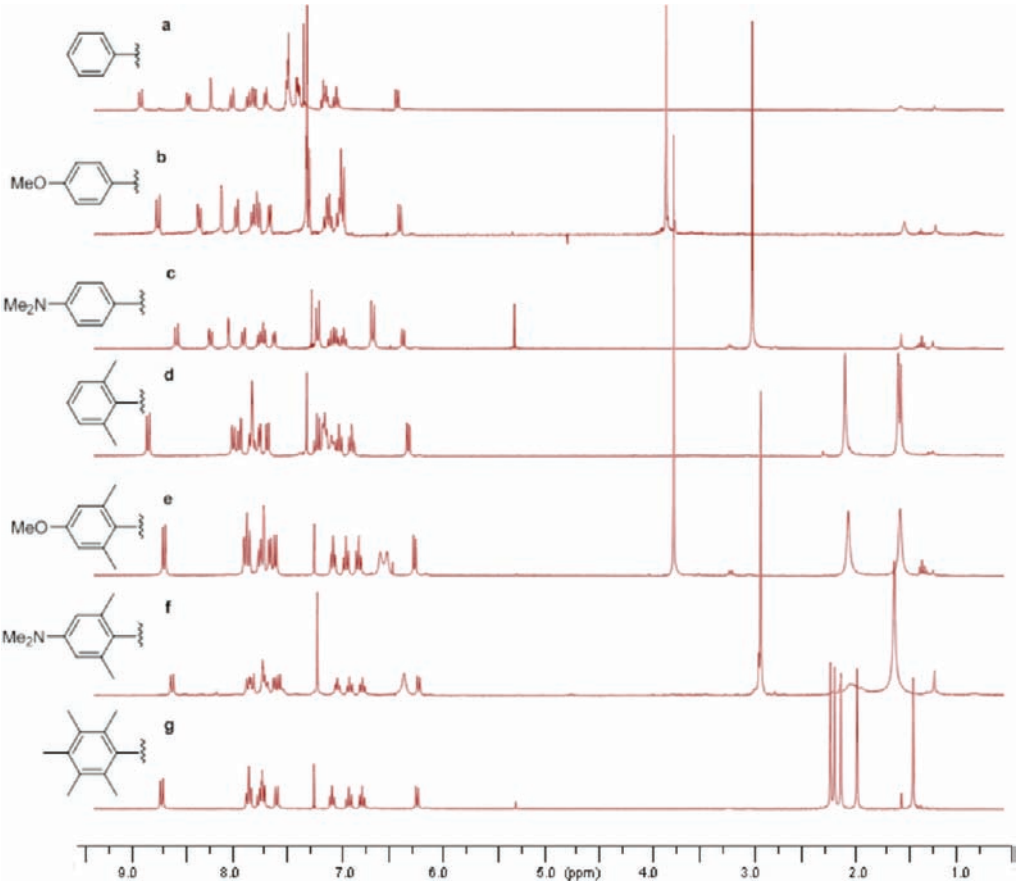

Figure 2. ^{1}H NMR spectra for **8a**−**8g** obtained in $CDCl_3$ at RT.

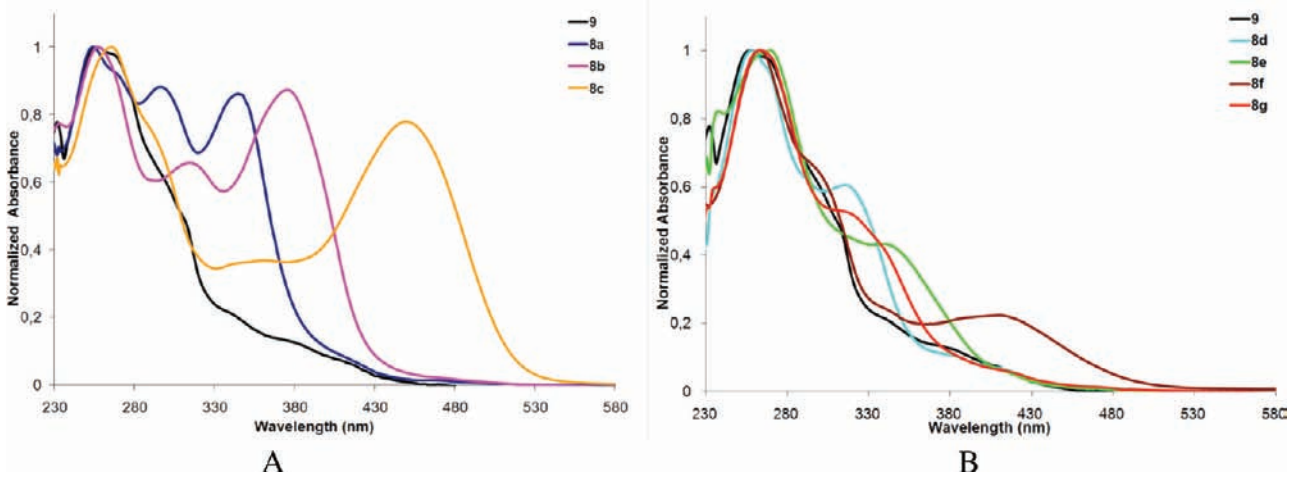

Figure 3. Normalized absorption spectra of (A) **8a**−**8c** and **9** and (B) **8d**−**8g** and **9** in 2-MeTHF at 298 K.

summarized in Table 2. The absorption spectrum for model complex **9** reproduces that found in the literature.[5i,14,28] Absorption spectra in 2-MeTHF for all complexes at RT showed the presence of an intense (ε on the order of 10^4−10^5 M^{-1} cm^{-1}) band between 254 and 266 nm, which was correlated to a spin-allowed ^{1}LC(ppy) π−π* transition.[1a,15a,b,29] Molar extinction coefficient values for **8a**−**8g** for the ^{1}LC and ^{1}MLCT transitions (see below) were found to be intense when compared to those in the literature. Classically, molar absorptivities are on the order of $(10-35) \times 10^3$ and $(2-6) \times 10^3$ M^{-1} cm^{-1} for π−π* and MLCT transitions, respectively.[14b,19,29a]

In the lower-energy region, well-defined spectra consisting of two additional peaks were observed for **8a**−**8c** (Figure 3A). These strongly absorbing bands were

(28) Plummer, E. A.; Hofstraat, J. W.; Cola, L. D. *Dalton Trans.* **2003**, 2080.

(29) (a) Ho, C.-L.; Wong, W. Y.; Zhou, G. J.; Yao, B.; Xie, Z.; Wang, L. *Adv. Funct. Mater.* **2007**, *17*, 2925. (b) Schmid, B.; Garces, F. O.; Watts, R. J. *Inorg. Chem.* **1994**, *33*, 9. (c) Ichimura, K.; Kobayashi, T.; King, K. A.; Watts, R. J. *J. Phys. Chem.* **1987**, *91*, 6104. (d) Colombo, M. G.; Hauser, A.; Güdel, H. U. *Top. Curr. Chem.* **1994**, *171*, 143.

Table 2. Photophysical Properties of Complexes **8a**−**8g** and **9**[a]

	absorbance at 298 K (nm) [molar absorptivities ($\times 10^4$ M^{-1} cm^{-1})]	phosphorescence (nm)		Stokes shifts (cm^{-1})		quantum yield (%)[c]	lifetime[d]		k_r ($\times 10^5$ s^{-1})	k_{nr} ($\times 10^5$ s^{-1})
		77 K[b]	298 K[b]	77 K	298 K		77 K (μs)	298 K (ns)		
9	256 [2.4], 270 [2.3], 300 [1.7], 344 [0.8], 380 [0.6], 415 [0.5]	532	595	5299	7290	6.2	(5.00)[e]	(269)[f]		
8a	254 [11.9], 266 [11.1], 297[10.6], 344 [10.3], 415 [0.9], 465 [0.2]	531	623	2673	5454	16.7	3.84	575	2.90	14.5
8b	254 [3.4], 315 [2.4], 375 [2.9]	551	613	8518	10353	21.2	7.26	934	2.27	8.40
8c	266 [6.0], 295 [2.2], 361 [2.2], 450 [4.6]	619	659	6067	7048	0.7	10.0	12.4	5.84	801
8d	258 [3.9], 316 [0.5], 379 [0.5], 410 [0.4], 471 [0.1]	516	599	1852	4537	22.0	3.97	668	3.29	11.7
8e	264 [4.0], 270 [4.0], 338 [2.0], 415 [0.3], 464 [0.02]	506	596	1789	4773	16.0	3.69	932	1.72	9.00
8f	266 [3.6], 304 [1.4], 418 [0.6], 442 [0.3], 488 [0.01]	563	613	2730	4179	2.0	3.76	508	0.39	19.3
8g	263 [5.4], 309 [2.8], 410 [0.4], 474 [0.04]	513	592	1604	4205	20.8	3.87	947	2.20	8.40

[a] Measured in 2-MeTHF. [b] λ_{max}. [c] In ACN ± 5%, using $Ru(bpy)_3(PF_6)_2$ as the standard (Φ = 6.2%). [d] Measured at λ_{max}; relative error ±5%. [e] From ref 41b in EtOH/MeOH glass. [f] From ref 3g.

assigned primarily to different ^{1}ILCT(bpy) $^1\pi-\pi^*$ transitions (270−360 and 344−450 nm).[3c,5d,g,14b,26a,29b,30] These assignments are corroborated by DFT/TD-DFT calculations (vide infra). As the donor availability of the group (X) on the bpy ligand increases from H to OMe to NMe_2, the energies of the second and third absorption bands are red-shifted and adhere to a free-energy relationship based on Hammett σ_p parameters (Figure S2 in the Supporting Information). Thus, an increasing bathochromic shift is observed with enlargement of the effective conjugative length of the ancillary ligand. De Cola and co-workers had recently reported a similar observation in the absorption spectra of a series of $[(dFppy)_2Ir[4\text{-}(n\text{-oligo}(p\text{-phenylene})]bpy)]^+$ complexes [dFppyH = 2-(2,4-difluorophenyl)pyridine; n = 0−3].[20] The characteristic ^{1}MLCT and ^{3}MLCT transitions[14b,15a,b,29d] found in $[(C^\wedge N)_2Ir(N^\wedge N)]^+$ complexes is masked by the more intense ^{1}ILCT transitions in these complexes.

In the case of complexes bearing *o*,*o*-dimethyl groups on the arene (**8d**−**8g**), the respective spectra display a primary ^{1}LC absorption at ca. 260 nm, with one or two additional moderate-to-weak absorption shoulders in a long tail between 304 and 470 nm. Within this low-absorption tailing region, the more intense peaks were assigned to an admixture of $^1\pi-\pi^*$ and ^{1}MLCT transitions, while less intense peaks were reasonably assigned to both a mixed $^3\pi-\pi^*$ and ^{3}MLCT transitions (Figure 3B)[3c,5g,31] and to geometrically forbidden ^{1}ILCT(bpy) $^1\pi-\pi^*$ transitions similar to those observed for, but exhibiting an order of magnitude lower molar absorptivity than, **8a**−**8c** (evidenced by TD-DFT calculations vide infra). The triplet spin-forbidden transitions are accessible because of the large spin−orbit coupling found in third-row heavy transition metals such as iridium.[15a,b,26a]

Emission. Emission spectra at low (77 K) and room (298 K) temperature were recorded for all of the complexes in deaerated 2-MeTHF solutions and are compiled in Table 2 and shown in Figures 4 and 5, respectively. Spectra obtained from measurements at 77 K in the glass state of 2-MeTHF frequently exhibited multiple emission maxima with emission energies (λ_{max}) ranging from green (506 nm) to red-orange (619 nm). Complexes **8a**−**8c** exhibited emission profiles different from those of **8d**−**8g**, with the latter resembling those determined for **9** (Figure 4). Note that, at this temperature, a single low-energy conformation essentially exists during spectral acquisition.

The fine structure of the emission spectra for **9** at 77 K (Figure 4B) has been attributed by Watts and co-workers as an indication of dual emission resulting from thermally nonequilibrated ^{3}MLCT excited states.[14a,19,32] Güdel and co-workers would later assert that the structured luminescence of $[(ppy)_2Ir(bpy)]^+$ originates from a mixed ^{3}MLCT and ^{3}LC(ppy) state.[29d] Thompson and co-workers[17e] more recently have advanced that the fine structure observed results from emission from different vibronic states of the excited species. The emission lifetimes for **8a**−**8g** at RT and 77 K could all be fitted to a mono-exponentially decaying function (vide infra), which would seem to preclude a dual-emission pathway. Thus, for each of **8a**−**8c**, three emission bands were readily observed and these were assigned to the different vibronic states of the ground-state species (Figure 4A). As with the absorption spectra, the emission energy (E_{em}) for **8a**−**8c** correlated well with the Hammett (σ_p) constants (Figure S2 in the Supporting Information); the emission lifetimes at 77 K were also found to increase from 3.84 to 10.0 μs with increasing donor ability of the aryl substituents and also were found to correlate linearly with the Hammett constants. The vibronic coupling between the ground and excited state, Δ [$=(2S_M)^{1/2}$, where S_M is the Huang−Rhys factor],[17e,33] and the dominant vibrational mode associated with the distortion between the ground and

(30) Maestri, M.; Balzani, V.; Deuschel-Cornioley, C.; von Zelewsky, A. *Adv. Photochem.* **1992**, *17*, 1.
(31) (a) Tamayo, A. B.; Alleyne, B. D.; Djurovich, P. I.; Lamansky, S.; Tsyba, I.; Ho, N. N.; Bau, R.; Thompson, M. E. *J. Am. Chem. Soc.* **2003**, *125*, 7377. (b) Polson, M.; Fracasso, S.; Bertolasi, V.; Ravaglia, M.; Scandola, F. *Inorg. Chem.* **2004**, *43*, 1950. (c) Neve, F.; Deda, M. L.; Puntoriero, F.; Campagna, S. *Inorg. Chim. Acta* **2006**, *359*, 1666. (d) Waern, J. B.; Desmarets, C.; Chamoreau, L.-M.; Amouri, H.; Barbieri, A.; Sabatini, C.; Ventura, B.; Barigelletti, F. *Inorg. Chem.* **2008**, *47*, 3340. (e) Bolink, H. J.; Coronado, E.; Costa, R. n. D.; Lardiés, N.; Orti, E. *Inorg. Chem.* **2008**, *47*, 9149.
(32) Wilde, A. P.; King, K. A.; Watts, R. J. *J. Phys. Chem.* **1991**, *95*, 629.
(33) Rillema, D. P.; Blanton, C. B.; Shaver, R. J.; Jackman, D. C.; Boldaji, M.; Bundy, S.; Worl, L. A.; Meyer, T. J. *Inorg. Chem.* **1992**, *31*, 1600.

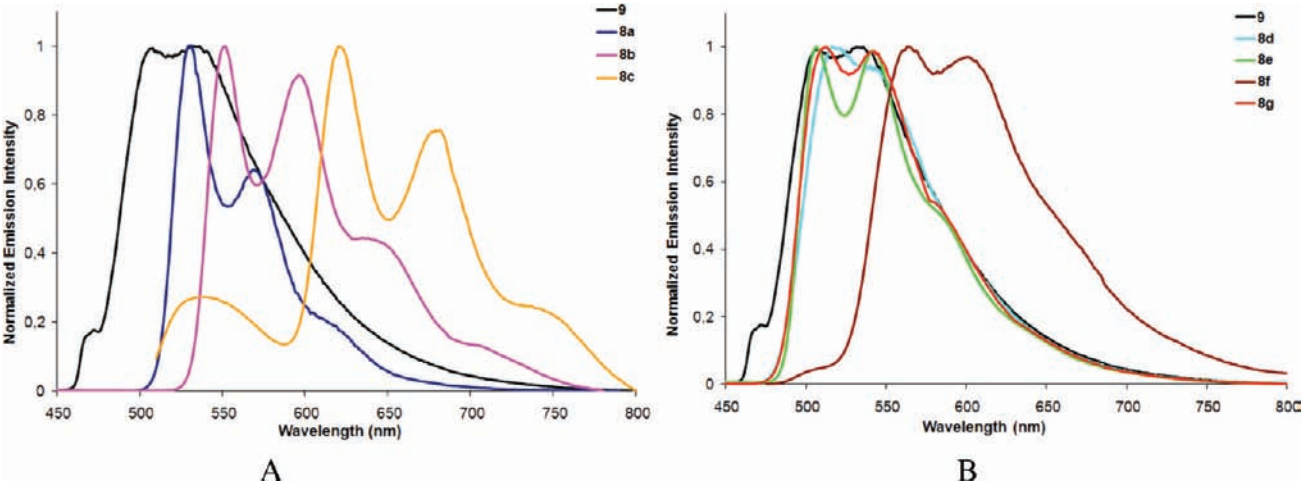

Figure 4. Normalized emission spectra of (A) **8a**−**8c** and (B) **8d**−**8g** and **9** in 2-MeTHF at 77 K.

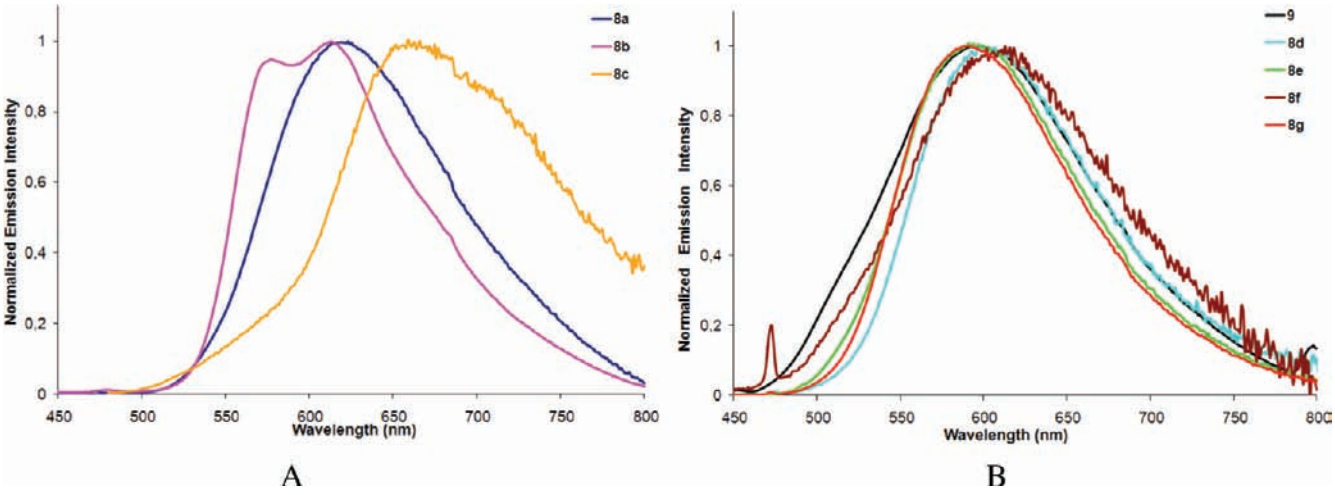

Figure 5. Normalized emission spectra of (A) **8a**−**8c** and (B) **8d**−**8g** and **9** in 2-MeTHF at 298 K.

excited states, ω, can be ascertained by modeling of the low-temperature emission spectra using the time-dependent theory of spectroscopy (Table 3 and eq S1 and Figures S3−S11 in the Supporting Information). The observed vibronic transitions (ω) correspond to the aromatic stretching modes of the aryl moiety[5i,17e,33] attached to the bpy but may also correspond to the bpy itself because it is also present in **9**.[5i,34] These assignments imply substantial contribution of the LLCT $\pi-\pi^*$ transition during emission and a much less significant contribution from the ^{3}MLCT state.[29a] Increased rigidity of the complex at low temperature might also contribute to the increased vibronic coupling.[35]

Complex **8c**, bearing the strongly electron-donating NMe_2 group, showed a fourth low-intensity, high-energy band at 537 nm before the characteristic vibronic emission pattern. We have attributed this peak to a fluorescence mechanism, assigned primarily because of the small observed Stokes shift. We were not able to confirm this assignment by independent lifetime measurements at λ_{max} for this band (537 nm) owing to the very low quantum yield of **8c**.[36] A possible explanation for its presence is through thermal repopulation of the singlet state in

Table 3. Calculated Excited-State Properties for **8a**−**8g** at 77 K[a]

complex	Δ^b	ω^c (cm^{-1})	$E_{0-0}{}^d$ (nm)
9	1.56	1320	505
18	1.25	1340	530
8b	1.53	1340	552
8c	1.39	1340	622
8d	1.47	1250	514
8e	1.56	1380	506
8f	1.54	1350	562
8g	1.54	1350	510

[a] The vibronic structure of the spectra was fitted to a first approximation on the basis of a single mode. See Supporting Information for a more complete description of these parameters. [b] Calculated horizontal offset between the ground and excited state minima along the normal coordinate at 77 K. [c] Calculated frequency of the vibrational mode at 77 K. [d] Obtained from the highest energy band at 77 K.

(34) (a) Yam, V. W.-W.; Tang, R. P.-L.; Wong, K. M.-C.; Lu, X.-X.; Cheung, K.-K.; Zhu, N. *Chem.—Eur. J.* **2002**, *8*, 4066. (b) Nakanishi, K.; Solomon, P. H. *Infrared Absorption Spectroscopy*, 2nd ed.; Holden-Day Inc.: San Francisco, 1977.

(35) Chen, H.-Y.; Yang, C.-H.; Chi, Y.; Cheng, Y.-M.; Yeh, Y.-S.; Chou, P.-T.; Hsieh, H.-Y.; Liu, C.-S.; Peng, S.-M.; Lee, G.-H. *Can. J. Chem.* **2006**, *84*, 309.

(36) Attempts to verify and further confirm the origin of the 537 nm band were not possible because of the weakly emissive nature of the compound that led to the poor signal-to-noise ratio of the excitation spectra.

phosphorescent species possessing long lifetimes (10 μs for **8c** at 77 K; see Table 2), a property that is not unprecedented.[37] The observed bathochromic shifts in the emission spectra within the series **8a**−**8c** were attributed to the incorporation of successively stronger electron-donating groups (**8a**, H; **8b**, OMe; **8c**, NMe_2) that upon initial analysis should effectively increase their conjugation lengths and thus should, according to classical frontier molecular orbital (FMO) theory, increase the energy of the HOMO and stabilize the LUMO.[38] As will be evidenced below, the arenes act, in fact, as electron-donating groups, destabilizing both the HOMO and LUMO, with an overall decrease in the HOMO−LUMO gap. The effect of substitution at the 4′ position of the aryls in **8a**−**8c** contrasts dramatically with those complexes studied by Neve and co-workers, which have the form $[(ppy)_2Ir(2\text{-phenyl-4-aryl-2,2}'\text{-bpy})]^+$.[26a] They observed a hypsochromic shift with increased donating ability of the remote substituents located at the 4′ position on the aryl ring. Thus, depending on the position of the aryl about the bpy chelate, the aryl can act either to decrease or increase the HOMO−LUMO gap.

The emission spectra at 77 K for **8d**−**8g**, which qualitatively appear similar to **9**, were hypsochromically shifted when compared to the analogous complexes within the series **8a**−**8c**, owing to the drastically diminished conjugation resulting from the orthogonal conformation of the arene relative to the bipyridine. The vibronic structure was evident within the series **8d**−**8g**, with two near-equal-intensity principle bands clearly observed (Δ in Table 3) as well as the presence of lower-energy shoulders. In general, Δ is similar in magnitude for both series of complexes, suggesting similar distortion profiles in the complexes.[17e,33]

Whereas the emission spectra at 77 K for **8a**−**8c** correlate well with the Hammett constants σ_p (Figure S2 in the Supporting Information), no analogous relationship was observed for **8d**−**8g**. All electronic communication is essentially cut because of the orthogonal disposition of the aryls with respect to the bpy plane, and there is essentially no difference in the emission energies of **8d**−**8g**, with the noticeable exception of **8f**; the lifetimes (τ_p) are also quite similar for this series, ranging from 3.7 to 4.0 μs (vide infra). A reasonable explanation for the observed exception in **8f** is the implication that the emissive transition occurs from distinct MOs that become accessible due to the increased electron density because of the inclusion of the NMe_2 electron-donating group. This hypothesis is corroborated by combined DFT/TD-DFT calculations (vide infra).

All of the complexes luminesced in solution at 298 K (Figure 5). Large Stokes shifts (4179−10353 cm^{-1}), measured from the lowest-energy absorption peak, reveal the expected phosphorescence in each of the seven complexes as well as in the reference, **9**. The emission maximum could be tuned marginally between 592 and 659 nm by varying the nature of the aryl. By comparison, **9** emits at 599 nm at 298 K in ACN. With the exception of **8b**, all complexes exhibited a single broad structureless emission band that was initially assigned to a ^{3}MLCT [dπ(Ir) → π*(bpy*)] excited state that is unremarkable in $[(C^\wedge N)_2Ir(N^\wedge N)]^+$-type complexes such as **9**.[5g,15a,b,29d,39] Analysis of the DFT/TD-DFT calculations (vide infra) has verified that the principle nature of the CT transitions is that of a mixed ^{3}LLCT/^{3}MLCT transition for **8a** and **8b**, while that of **8c** is a ^{3}ILCT transition. Surprisingly, dual emission with strong bands at 577 and 613 nm was observed from **8b**. Given that the lifetimes at each of these two emission wavelengths were found to be distinct but invariant to changes in the concentration and given that the excitation spectra obtained at each of these two wavelengths were found to be superimposable, a reasonable hypothesis is that the dual emission observed arises from two distinct conformations in solution at RT.

Emission maxima (E_{max}) at RT for all complexes were significantly bathochromically shifted compared to E_{max} from spectra obtained at 77 K. At RT, rapid reorganization of the solvent molecules can stabilize CT states prior to emission, a process that is encumbered in viscous media or a rigid matrix at low temperatures.[3n,8,40] The particularly large blue shift observed upon cooling is indicative that emission occurs, in part, from a ^{3}CT state.[3n] The trends relating to the emission energies observed at 77 K do not exist at RT, ostensibly because of the existence of differing dynamic conformations that are certainly operative for **8a**−**8c**.

As with **9**, the emission spectra for **8d**−**8g** at 298 K were generally broad and featureless, with emission maxima at 599, 596, 613, and 592 nm for **8d**−**8g**, respectively (Figure 5B). Unlike **8a**−**8c**, essentially no bathochromic shift was observed, the explanation of which originates from the electronic decoupling of the aryl groups from the bpy. No trend could be ascertained between the character of the arene and the emission energy for either series (i.e., **8a**−**8c** or **8d**−**8g**). The small energy tuning effect for the latter series (592−613 nm; cf. Table 2) can be explained by the loss of conjugation between the aryl and the bpy plane.[26d] Thus, all complexes in this series seem to exhibit emission spectra essentially similar to that found for **9** and are bathochromically shifted when compared with complexes bearing inductively electron-donating groups such as $[(ppy)_2Ir(5,5'\text{-dmbpy})]^+$ (λ_{em} = 570 nm, Φ = 18%, τ = 0.5 μs; 5,5′-dmbpy = 5,5′-dimethyl-2,2′-bipyridine).[3g] With the exception of **8f**, the emission for **8d**−**8g** was attributed to originate from an admixture of ^{3}LLCT and ^{3}MLCT excited states, similar to that found for **8a**, **8b**, and **9**.[3d,15a] The small bathochromic shift (ca. 20 nm) observed for **8f** compared to those of the other complexes in the series can be rationalized through an ^{3}ILCT emissive transition, similar to that found for **8c**. These assignments were corroborated by DFT/TD-DFT (vide infra).

Photoluminescent Quantum Yields and Lifetimes. Quantum yields (Φ_p) for **8a**−**8g** solutions in deaerated ACN at RT ranged from 1 to 22%. With the exception of

(37) (a) Liu, Y.; Jiang, S.; Glusac, K.; Powell, D. H.; Anderson, D. F.; Schanze, K. S. *J. Am. Chem. Soc.* **2002**, *124*, 12412. (b) Turro, N. J. *Modern Molecular Photochemistry*; University Science Books: Sausalito, CA, 1991.

(38) (a) Mak, C. S. K.; Hayer, A.; Pascu, S. I.; Watkins, S. E.; Holmes, A. B.; Kohler, A.; Friend, R. H. *Chem. Commun.* **2005**, 4708. (b) Fleming, I. *Frontier Orbitals and Organic Chemical Reactions*; John Wiley & Sons: Toronto, Ontario, Canada, 1976.

(39) Dragonetti, C.; Falciola, L.; Mussini, P.; Righetto, S.; Roberto, D.; Ugo, R.; Valore, A.; De Angelis, F.; Fantacci, S.; Sgamellotti, A.; Ramon, M.; Muccini, M. *Inorg. Chem.* **2007**, *46*, 8533.

(40) Juris, A.; Balzani, V.; Barigelletti, F.; Campagna, S.; Belser, P.; von Zelewsky, A. *Coord. Chem. Rev.* **1988**, *84*, 85.

complexes bearing NMe_2 groups (**8c** and **8f**) that exhibit particularly weak phosphorescence ($\Phi_p \sim 1\%$), these complexes are remarkably bright ($\Phi_p = 16-22\%$; Table 2) compared to similar complexes bearing extended π-conjugated frameworks found in the literature.[3l,n,aa,26a,c,d,31c,41] Even arguably, some of the best yellow-to-orange emitters used in single-layer devices, $[(ppy)_2Ir(dtb\text{-}bpy)]PF_6$[3e,42] and $[(ppy)_2Ir(sb)]PF_6$[3l] (dtb-bpy = 4,4′-di-*tert*-butylbipyridine; sb = 4,5-diaza-9,9′-spirobifluorene), which luminesce at 581 and 605 nm in ACN with quantum yields of 23.5% and 22.6% and lifetimes of 557 and 330 ns, respectively, have photophysical characteristics essentially similar to those found in this study. Bolink and co-workers have, in fact, recently shown that aryls appended onto the ancillary diimine decrease nonradiative intermolecular charge recombination through steric shielding of the iridium center.[3d] Thus, it is gratifying to observe that similar photophysical characteristics exist for most of the complexes in this study.

By contrast, the lower-energy emission at RT coupled with shorter observed lifetimes (τ_p), particularly for **8c** (τ_p = 12.4 ns), results in much lower quantum yields (0.7% for **8c**; 2.0% for **8f**) and, accordingly, large calculated nonradiative decay rate constants (k_{nr}). The surprising marked decrease in the emission intensity implies a new radiationless pathway operative in **8c** and **8f**, due to the presence of distinctly electron-rich aniline substituents. The increased conjugation imparted by the presence of NMe_2 groups facilitates greatly nonradiative electron transfer in the excited state for **8c**. Owing to the orthogonal orientation of the arene, **8f** does not succumb so readily to this deactivation pathway and so possesses relatively longer-lived phosphorescence. Pendant alkylamines,[5c] alkylammonium salts,[3y] or amines directly substituted onto the ancillary ligand[3c,5d] of heteroleptic iridium complexes do not substantially impact the emission intensity; exceptionally, $[(ppy)_2Ir(5\text{-}NMe_2\text{-}1,10\text{-}phen)]^+$ exhibited a quantum yield of only 0.3% in dichloromethane (DCM).[39]

Observed phosphorescent lifetime (τ_p) values at RT in 2-MeTHF were modeled as single-exponential decays and are on the nanosecond-to-submicrosecond time scale (12.4−934 ns), values generally not dissimilar to other cationic iridium(III) complexes[3g,14a,31c,39] but generally 2−4 times longer than that found for **9**.[18] The long-lived emission is a further indication of a phosphorescence radiative pathway.[29c] With measured τ_p and Φ_p data in hand, the radiative and nonradiative rate constants (k_r and k_{nr}) were calculated with eqs 1 and 2, respectively. The values for the radiative rate constant (k_r) are quite similar for **8a**−**8g**, are on the order of 10^5 s^{-1}, and are similar to those previously reported by Mussini et al.[39] The limiting factor that seems to control the quantum yield in **8a**−**8g** is the nonradiative rate constant (k_{nr}), for

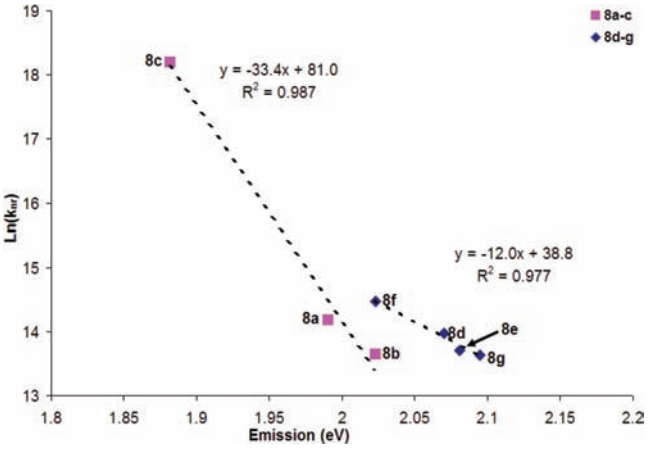

Figure 6. $\ln(k_{nr})$ vs emission energy (E_{em}) at 298 K in 2-MeTHF for **8a**−**8c** (pink ■) and **8d**−**8g** (blue ◆). The dashed lines represent linear least-squares fits to the data.

which we observe a significantly larger variation, with values ranging from 10^5 to 10^7 s^{-1}. This range is much larger than the one reported by the previous group (from 1.6 to 7.1 × 10^5 s^{-1}), and the difference may be attributed to the loss of rigidity due to migration from a phenanthroline to a bipyridine ligand architecture. Surprisingly, the relaxation dynamics of **8a** and **8b**, which possess freely rotating aryl groups, are not adversely affected when compared to their dimethylated congeners (**8d**−**8e**).

$$k_r = \frac{\Phi_p}{\tau_p} \quad (1)$$

$$k_{nr} = \frac{1-\Phi_p}{\tau_p} \quad (2)$$

Both series of isostructural complexes obey the energy gap law[21] at RT when analyzed independently (Figure 6) in accordance with other iridium(III) luminophores.[17e,26a,43] The fact that there is such a linear fit would seem to indicate that the excited states for **8a**−**8c** are similar while those for **8d**−**8g** are comparable, at least as far as deactivation dynamics are concerned. The calculated slope of −12.02 eV^{-1} for the series comprising **8d**−**8g** is similar to that found for other polypyridine complexes such as tricarbonyl(bipyridine)rhenium(I) complexes whose values range from −9.0 to −11.9 eV^{-1} in ACN.[44] By contrast, the calculated slope for **8a**−**8c** is significantly larger. This is almost certainly an artifact due to a paucity of data points coupled with the significant red shift observed for **8c**. A reasonable supposition, given that **8c** emits via a pathway distinct from **8a** and **8b** but similar to **8f**, is that their deactivation dynamics are also different.

Solvatochromic Study. For each of **8a**−**8g**, absorption and emission spectra obtained in either 2-MeTHF or ACN were found to be superimposable. The apparent lack of solvent dependence was surprising given the CT nature of the observed transition and thus led us to

(41) (a) Cunningham, G. B.; Li, Y.; Liu, S.; Schanze, K. S. *J. Phys. Chem. B* **2003**, *107*, 12569. (b) Glusac, K. D.; Jiang, S.; Schanze, K. S. *Chem. Commun.* **2002**, 2504. (c) Kim, K.-Y.; Farley, R. T.; Schanze, K. S. *J. Phys. Chem. B* **2006**, *110*, 17302. (d) Zeng, X.; Tavasli, M.; Perepichka, I. F.; Batsanov, A. S.; Bryce, M. R.; Chiang, C.-J.; Rothe, C.; Monkman, A. P. *Chem.—Eur. J.* **2008**, *14*, 933. (e) Zhao, Q.; Liu, S.; Shi, M.; Wang, C.; Yu, M.; Li, L.; Li, F.; Yi, T.; Huang, C. *Inorg. Chem.* **2006**, *45*, 6152. (f) Rothe, C.; Chiang, C.-J.; Jankus, V.; Abdullah, K.; Zeng, X.; Jitchati, R.; Batsanov, A. S.; Bryce, M. R.; Monkman, A. P. *Adv. Funct. Mater.* **2009**, *19*, 2038.

(42) Parker, S. T.; Slinker, J. D.; Lowry, M. S.; Cox, M. P.; Bernhard, S.; Malliaras, G. G. *Chem. Mater.* **2005**, *17*, 3187.

(43) Siebrand, W. *J. Chem. Phys.* **1967**, *46*, 440.

(44) (a) Caspar, J. V.; Westmoreland, T. D.; Allen, G. H.; Bradley, P. G.; Meyer, T. J.; Woodruff, W. H. *J. Am. Chem. Soc.* **1984**, *106*, 3492. (b) Baiano, J. A.; Murphy, W. R. *Inorg. Chem.* **1991**, *30*, 4594.

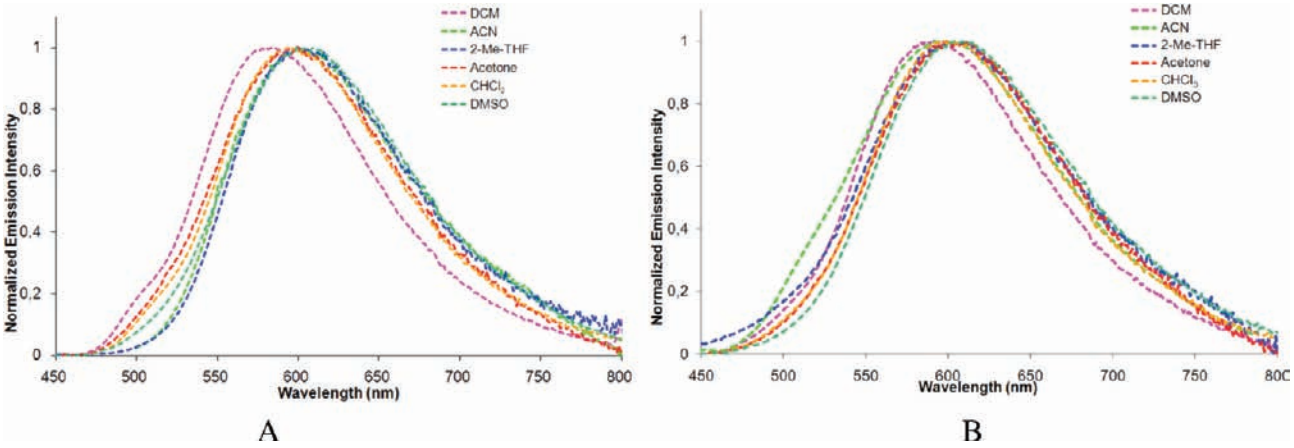

Figure 7. Normalized emission spectra for (A) **8d** and (B) **9** at 298 K in different solvents.

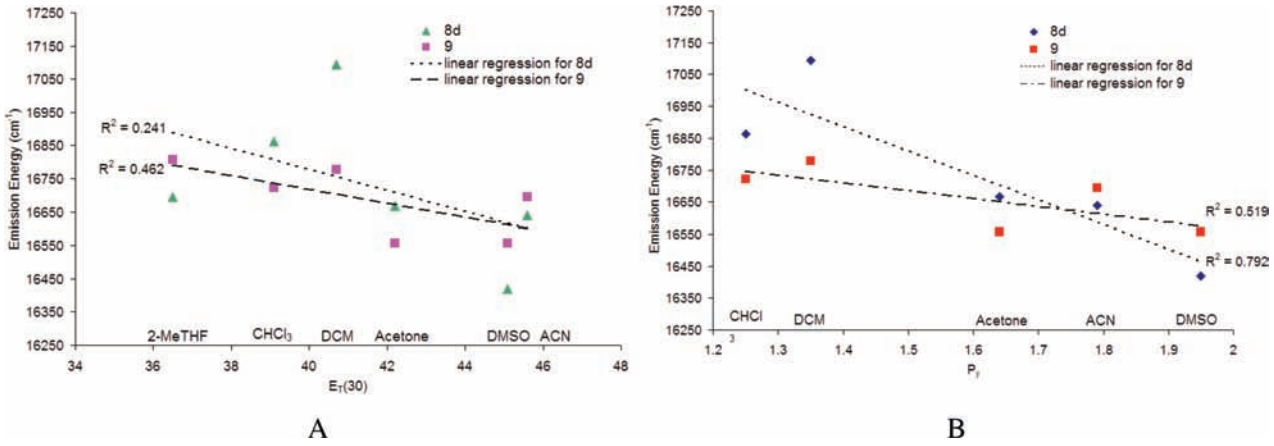

Figure 8. Correlation diagram for the emission energy with (A) Reichardt−Dimroth solvent $E_T(30)$ parameters and (B) a Winnik−Dong solvent P_y scale for **8d** (blue ◆) and **9** (red ■).

investigate more closely solvatochromism in **8d**, as a prototypical complex of the family under investigation, and compare its behavior to **9**. The emission spectra for **8d** and **9** were obtained in six solvents of disparate polarity and identity (Figures 7 and 8). Inspection of the emission maximum as a function of the solvent polarity, as measured by the Reichardt−Dimroth[45] solvent polarity function [$E_T(30)$] or the P_y scale developed by Winnik and Dong,[46] suggests that, in fact, both complexes are moderately solvatochromic (Figure 8 and Table 4). In general, polar solvents stabilized the dipole−dipole interaction of the excited state, shifting the emission spectrum to the red.[47] No clear linear correlation could be obtained for **9**; however, there is an observed solvatochromic sensitivity[5g,15b] of the ^{3}MLCT transition, in agreement with that found by Watts and co-workers (Figure 8).[47b] A similar monotonic correlation could be ascertained between $E_T(30)$ or P_y and λ_{max} for **8d**.[48]

Electrochemical Characterization. Electrochemical analysis via cyclic voltammetry (CV) was performed in order to measure the redox potentials of **8a**−**8g** and **9**. The electrochemical data are summarized in Table 5. The reversible cyclic voltammogram for **9**, acquired as an ACN solution with 0.1 M of tetra-*n*-butylammonium hexafluorophosphate ($TBAPF_6$) as the supporting electrolyte at 298 K, exhibits an oxidation couple at 1.44 V and a reduction couple at −1.32 V (ΔE_{red-ox} = 2.76 V; $\Delta_{red-ox} = E^{ox}_{pa} - E^{red}_{pc}$). The CV accurately reproduces, although is slightly cathodically shifted to, that reported in the literature (E^{ox}_p = 1.25 V; E^{red}_p = −1.42 V; Δ_{red-ox} = 2.67 V)[4b] and is in good agreement with the theoretical value calculated for this complex (2.75 eV, vide infra). The first oxidation wave for **9** has been mainly attributed to a metal center Ir^{IV}/Ir^{III} couple, with substantial contributions from the cyclometalating ppy ligands. Generally, metal-centered oxidation is assumed to be a completely reversible process, with the degree of irreversibility increasing with an increase in the contribution of the ppy ligand to the electron density distibution of the HOMO.[26a,39,41e,49] The first reduction wave has been assigned to a localized

(45) Reichardt, C. *Chem. Rev.* **1994**, *94*, 2319.
(46) Dong, D. C.; Winnik, M. A. *Can. J. Chem.* **1984**, *62*, 2560.
(47) (a) Lo, K. K.-W.; Lau, J. S.-Y.; Lo, D. K.-K.; Lo, L. T.-L. *Eur. J. Inorg. Chem.* **2006**, *2006*, 4054. (b) Wilde, A. P.; Watts, R. J. *J. Phys. Chem.* **1991**, *95*, 622.
(48) It is frequently difficult to ascertain the magnitude and origin of the solvatochromism in complexes of the type $[(C^N)_2Ir(N^N)]^+$. For instance, λ_{max} for emission in ACN for **9** has been measured to be 580,[31b] 583,[3g] 585,[3y] and 588 nm;[3s] additionally, λ_{max} for emission for the chloride salt of **9** has been measured to be 616 nm.[23b]
(49) (a) Didier, P.; Ortmans, I.; Kirsch-De Mesmaeker, A.; Watts, R. J. *Inorg. Chem.* **1993**, *32*, 5239. (b) Calogero, G.; Giuffrida, G.; Serroni, S.; Ricevuto, V.; Campagna, S. *Inorg. Chem.* **1995**, *34*, 541. (c) Neve, F.; Crispini, A.; Serroni, S.; Loiseau, F.; Campagna, S. *Inorg. Chem.* **2001**, *40*, 1093.

Table 4. Solvent-Induced Shifts in Emission Maxima for **8d** and **9**

			emission energy [cm^{-1} (nm)]			
			8d	**9**		
solvent	$E_T(30)$ (kcal/mol)	P_y	this study	lit.		ref
2-MeTHF	36.5		16 695 (599)	16 807 (595)		*a*
THF	37.4	1.35			16 949 (590)	41b
$CHCl_3$	39.1	1.25	16 863 (593)	16 722 (598)	16 667 (600)	47b[b]
DCM	40.7	1.35	17 094 (585)	16 779 (596)	16 750 (597)	47b[b]
acetone	42.2	1.64	16 667 (600)	16 556 (604)	16 556 (604)	47b[b]
DMSO	45.1	1.95	16 420 (609)	16 556 (604)	16 556 (604)	47b[b]
ACN	45.6	1.79	16 639 (601)	16 695 (599)	17 007 (588)	5i
MeOH	55.4	1.35			16 502 (606)	5i

[a] No data reported in the literature. [b] The measurement was obtained from the chloride salt of **9**.

Table 5. Redox Properties for **8a**−**8g** and **9**[a,b]

	oxidation										reduction								
				Ir^{IV}/Ir^{III}							bpy			ppy					
	E_{pa}	E_{pc}	ΔE	E_{pa}	E_{pc}	ΔE	E_{pa}	E_{pc}	ΔE	ΔE_{red-ox}	E_{pa}	E_{pc}	ΔE	E_{pa}	E_{pc}	ΔE	E_{pa}	E_{pc}	ΔE
9	2.20	2.04	0.15[c]	1.44	1.27	0.17[c]				2.76	−1.30	−1.32	0.02[c]	−2.01	−2.04	0.03[c]	−2.17	−2.29	0.12[c]
8a	2.13		[e]	1.34	1.31	0.03[c]				2.61	−1.19	−1.27	0.08[c]	−1.69	−1.79	0.10[c]			
8b	1.94		[e]	1.38	1.27	0.11[c]				2.66	−1.22	−1.29	0.06[c]	−1.76	−1.85	0.09[c]			
8c				1.44	1.33	0.11[c]	1.03	0.88	0.15[d]	2.44	−1.27	−1.41	0.14[c]	−1.85	−1.93	0.08[c]			
8d	2.27		[e]	1.42	1.26	0.16[c]				2.76	−1.26	−1.33	0.08[c]	−1.91	−1.99	0.08[c]			
8e	1.90		[e]	1.37		[e]				2.77	−1.27	−1.40	0.13[d]						
8f				1.46		[e]	0.97		[e]	2.39	−1.34	−1.42	0.08[c]	−2.10	−1.99	0.11[d]			
8g	2.05		[e]	1.39	1.32	0.08[c]				2.67	−1.30	−1.36	0.06[c]	−1.97	−2.07	0.10[c]			

[a] CV was carried out at 100 mV/s in 0.1 M $TBAPF_6/CH_3CN$ at a platinum working electrode with glassy carbon as the counter electrode and an Ag/Ag^+ electrode as a pseudoreference. Ferrocene was used as an internal standard, and potentials are reported with respect to a saturated calomel electrode (SCE). [b] E_{pa} and E_{pc} correspond to anodic and cathodic peak potentials (V), and ΔE is the difference calculated between these two potentials. ΔE_{red-ox} is the difference between the smaller E_{pa} and the biggest E_{pc} values (V). Values are evaluated with a 10% relative error. [c] Refers to a reversible process. [d] Refers to a quasi-reversible process. [e] Refers to an irreversible process.

reduction of the bpy ligand, while the second reduction wave is assigned to the localized reduction of the ppy ligand. These assignments match those previously reported and are also consistent with DFT calculations (vide infra).[3c,n,14,39,50]

The following observations were made with respect to the CVs of **8a**−**8g** (cf. Figures S12−S13 in the Supporting Information) regardless of the scan rate (50−200 mV/s). Compared to **9**, the first oxidation potentials for each of **8a**, **8d**, and **8g** are anodically shifted by 100, 20, and 50 mV, respectively, and were found to be reversible. Similar to **9**, this first oxidation wave was attributed to a one-electron oxidation eminating from a combined metal phenylpyridine MO. A second irreversible oxidation wave at 2.20, 2.27, and 2.05 V for **8a**, **8d**, and **8g**, respectively, was also detected. The irreversibility of this second oxidation peak distinguishes these three complexes from **9**, which was found to be reversible.

Their respective first reduction peak potentials are also reversible, with **8a** being cathodically shifted by 50 mV and **8d** and **8g** being anodically shifted by 10 and 40 mV, respectively, relative to **9**. The first reduction potential corresponds to the energy of the LUMO, which is localized on the diimine as ascertained by computations (vide infra). The larger cathodic shift for **8a** is attributed to the greater conjugative influence compared to the more orthogonally oriented arenes found in **8d** and **8g**, which should result in a lowering of the energy of the LUMO for the former. Accordingly, there is an overall decrease in the HOMO−LUMO energy gap (ΔE_{red-ox}) for **8a** to 2.61 V, while the energy gap remains essentially unchanged at 2.76 and 2.67 V for **8d** and **8g**, respectively. This decrease in the HOMO−LUMO energy gap is not generally reproduced computationally, the results of which indicate a tiny blue shift. Additionally, each of these complexes exhibit two additional reversible or quasi-reversible reduction waves between −1.79 and −2.05 V, which have been assigned to successive reductions of the cyclometalating ppyH.[5c,d,26a,d]

The CV traces for **8b** and **8c** exhibit reversible oxidation peaks for metal-centered orbitals with contributions from the cyclometalating ppyH at 1.38 and 1.44 V, respectively, that are only slightly anodically shifted compared to that of **9**. Additionally, **8c** possesses a second oxidation peak at 1.03 V that has been attributed to oxidation of the aniline fragment, a conclusion consistent with DFT calculations (vide infra). The quasi-reversible oxidation peak for **8b** observed at 1.94 V is attributed to oxidation of the anisole fragment based on analysis of the MOs from DFT calculations, below. Each displays two reduction peak potentials that are generally slightly cathodically shifted with respect to **9**; the first reduction peak for **8c** is anodically shifted by 90 mV. As such, ΔE_{red-ox} for **8c** is significantly smaller at 2.44 V than that found for **8b** (2.66 V). Overall, the HOMO−LUMO energy gap for

(50) (a) Bandini, M.; Bianchi, M.; Valenti, G.; Piccinelli, F.; Paolucci, F.; Monari, M.; Umani-Ronchi, A.; Marcaccio, M. *Inorg. Chem.* **2010**, *49*, 1439. (b) Stagni, S.; Colella, S.; Palazzi, A.; Valenti, G.; Zacchini, S.; Paolucci, F.; Marcaccio, M.; Albuquerque, R. Q.; De Cola, L. *Inorg. Chem.* **2008**, *47*, 10509.

Table 6. Comparison of Measured and Calculated Ground-State Geometries for **8a**

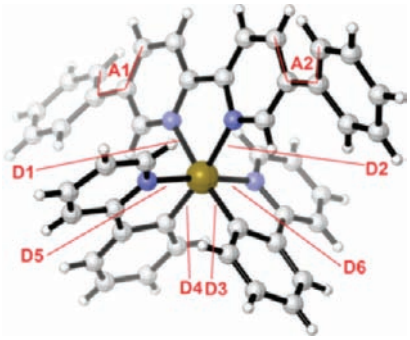

	experimental structure		calculated structure					
structural parameter	crystal structure	uncertainty (%)	method 1[a]	relative error (%)[b]	method 2[c]	relative error (%)[b]	method 3[d]	relative error (%)[b]
A1 (deg)	32 ± 3.0	9	35	9	27	15	37	15
A2 (deg)	37 ± 1.7	5	36	3	23	37	37	0
D1 (Å)	2.146 ± 0.009	0.4	2.214	3.2	2.180	15.8	2.165	0.9
D2 (Å)	2.121 ± 0.010	0.5	2.211	4.2	2.179	2.7	2.165	2.1
D3 (Å)	1.985 ± 0.012	0.6	2.022	1.9	2.035	2.5	2.039	2.7
D4 (Å)	2.002 ± 0.012	0.6	2.022	1.0	2.039	1.8	2.039	1.8
D5 (Å)	2.041 ± 0.010	0.5	2.081	2.0	2.078	1.8	2.074	1.6
D6 (Å)	2.053 ± 0.011	0.5	2.081	1.4	2.082	1.4	2.074	1.0

[a] *Gaussian 03*: B3LYP/6-31+G* for C, H, N, and O; B3LYP/LAN2DZ for Ir. [b] Relative error between the optimized and X-ray structures. [c] *Gamess*: B3LYP/SBKJC-31G for C, H, N, O, and Ir. [d] *Gaussian 03*: B3LYP/3-21G* for C, H, N, and O; B3LYP/SBKJC-VDZ for Ir.

8a−**8c** decreases from **8b** > **8a** > **8c**, a trend that mirrors that observed for emission at 298 K (cf. Figure 5).

The behavior of the CV traces for **8e** and **8f** is different. For **8f**, two quasi-reversible oxidation peaks at 0.97 and 1.46 V were observed, similar to that found for **8c**. DFT calculations place the HOMOs for **8c** and **8f** on the aniline fragment of the diimine (vide infra). Unfortunately, although **8e** was found to be highly phosphorescent, because of exhibition of an irreversible oxidation wave, this complex does not seem to be a good candidate for device fabrication. The lack of reversibility observed for the oxidation waves has, in other heteroleptic iridium complex systems, been attributed to an increased contribution of the cyclometalating ligand via augmented covalent σ(Ir−C) character in the HOMO, resulting in its destabilization.[3n,26d,41e,49a,51] This is not the case here because we observe a net yet small stabilization of the HOMO by CV. The quasi-reversible nature of the first reduction wave for **8e** suggests that the anisole fragment is somewhat involved in the reduction process. The first reduction peak for **8f**, on the other hand, was found to be reversible. This first reduction peak is anodically shifted by 80 and 100 mV for **8e** and **8f**, respectively. For the moment, we have no satisfactory explanation for the difference of behavior between **8e** and **8f**.

According to the CVs, the overall impact for the inclusion of aryl groups on the bpy ligand is to destabilize the HOMO relative to **9**. There did not seem to be a general trend in terms of the magnitude of this destabilization, but this behavior is corroborated by the computational predictions. For **8c** and **8f**, there is a substantial reduction in the HOMO−LUMO gap. This red shift was also observed spectroscopically (vide supra). The radical cation on the aniline results in a large net destabilization of the HOMO in these two complexes. The remainder of the complexes exhibited a destabilization of the HOMO associated with the Ir^{IV}/Ir^{III} couple. With the exception of **8a** and **8b**, their corresponding LUMO energies, as measured as E_{pc} of the first reduction peak, were found to be anodically shifted and their destabilization is of a magnitude comparable to that found for the destabilization of the HOMO, resulting in an overall slight decrease in the HOMO−LUMO gap compared to **9**. A more detailed investigation into the electrochemical properties is ongoing and will be reported elsewhere.

Computational Modeling Approaches. Recently, several groups have employed computations as a tool for the prediction and modeling of the photophysical properties of luminescent organometallic complexes.[3g,17a,b,e,f,18,31b,39,50a,52] In order to obtain accurate photophysical property predictions, a rigorous methodology must be established. First, the ground- and excited-state geometries must be modeled accurately[53] because these will directly impact accurate absorption and emission energy predictions. In our current work, theoretical predictions of the photophysical properties of **8a**−**8g** and **9** were obtained through a combined TD-DFT/DFT study (cf. Tables S4−S11 in the Supporting Information). We employed DFT methods using the B3LYP functional with low-cost basis sets (3-21G*) used

(51) Serroni, S.; Juris, A.; Campagna, S.; Venturi, M.; Denti, G.; Balzani, V. *J. Am. Chem. Soc.* **1994**, *116*, 9086.

(52) (a) Bolink, H. J.; Cappelli, L.; Cheylan, S.; Coronado, E.; Costa, R. D.; Lardies, N.; Nazeeruddin, M. K.; Orti, E. *J. Mater. Chem.* **2007**, *17*, 5032. (b) Di Censo, D.; Fantacci, S.; De Angelis, F.; Klein, C.; Evans, N.; Kalyanasundaram, K.; Bolink, H. J.; Gratzel, M.; Nazeeruddin, M. K. *Inorg. Chem.* **2008**, *47*, 980. (c) Velusamy, M.; Thomas, K. R. J.; Chen, C.-H.; Lin, J. T.; Wen, Y. S.; Hsieh, W.-T.; Lai, C.-H.; Chou, P.-T. *Dalton Trans.* **2007**, 3025.

(53) Predicted ground-state geometries are deemed accurate if the structural parameters fall within 1 standard deviation of the experiment.

to model carbon, hydrogen, nitrogen, and oxygen centers, while the SBKJC-VDZ basis set was used to model the iridium center (method 3, Table 6). We then compared our predicted geometries to two other methods commonly used in the literature.

As an example of the effectiveness of method 3, selected measured and calculated ground-state structural parameters for **8a** are compared within Table 6. Ir−N(bpy), Ir−N(ppy), and Ir−C(ppy) distances for **8a** were calculated to be 2.17, 2.04, and 2.07 Å, respectively, which slightly overestimate distances of 2.13, 1.99, and 2.04 Å, respectively, found in the X-ray structure; other bond lengths and bond and dihedral angles were, in general, also accurately reproduced. This combined protocol proved to be a more accurate predictor of the geometry for complexes such as **8a** at far smaller computational cost than the most commonly used computational method found in the literature for these types of complexes, namely, the B3LYP[54] functional with the 6-31+G* Pople[55] double-ζ split valence basis set for carbon, hydrogen, oxygen, and nitrogen and LANL2DZ[56] for iridium (method 1, Table 6). This latter method overestimated the bond lengths by 1−4%; however, it did slightly more accurately predict the dihedral angles found in the X-ray structure than method 3 did. The use of the SBKJC-31G[57] basis set for all atoms within *Gamess*[58] (method 2, Table 6) proved even less effective, severely underestimating the dihedral angles formed by the intersection of the arene and bpy planes. Calculated excited state (T_1) bond lengths using method 3 mirror those found in the ground state with only ca. 1% contraction observed (cf. Table S2 in the Supporting Information). Generally, there is a slight planarization observed in the triplet state for both ligands: the two pyridines in bpy and the phenyl and pyridine in ppyH become more coplanar. Dihedral angles between the arene and the bpy plane for **8a**−**8g** diminish from 1 to 43%. Complexes bearing methoxy groups on the arene (**8b** and **8e**) were found to exhibit the greatest conformational change within each series.

With ground-state structure prediction sound, we turned our attention toward an examination of the torsional potentials for the C_{aryl}−C_{bpy} bond for each of **8a**, **8d**, and **8g** in an effort to explain the observed anisochronous

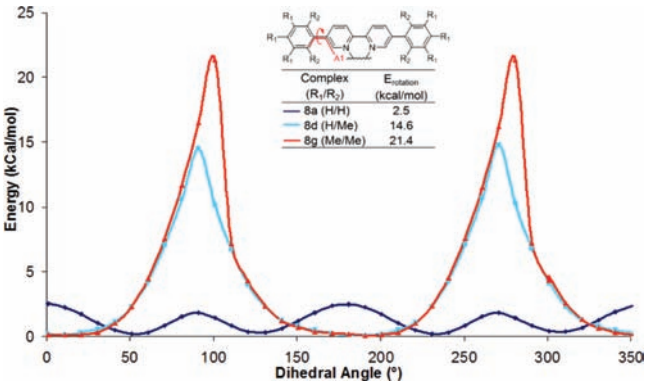

Figure 9. Calculated rotational barriers about the C_{aryl}−C_{bpy} bond.

methyl signals in the ^{1}H NMR spectra for the latter two complexes. We performed a relaxed dihedral potential energy scan using our validated method 3. The rotational barriers for **8a**, **8d**, and **8g** were calculated to be 2.5, 14.6, and 21.4 kcal/mol, respectively (Figure 9). The barrier for **8a** is similar to that found for biphenyl (exptl,[59] 1.4 kcal/mol; calcd at MP2/cc-pV∞Z,[60] 2.2 kcal/mol; calcd at CC-cf,[61] 1.9 kcal/mol), while that for **8d** is significantly smaller than that determined for 2,6-dimethylbiphenyl (exptl,[62] >23.9 kcal/mol). Rotation about the C_{aryl}−C_{bpy} bond in **8g** is calculated to be further restricted (21.4 kcal/mol) because of steric interactions between the methyl groups found meta to this bond and the remainder of the ligand framework about the complex. The elevated calculated rotational barriers for **8d** and **8g** plausibly explain the observed atropisomerism evident in the ^{1}H NMR spectra (vide supra).

Following accurate geometry optimization, we next modeled the electronic structure of each of the complexes. TD-DFT calculations are particularly amenable to providing insight into the different singlet and triplet excited states, which can be related to absorption and emission processes, respectively. TD-DFT has of late become increasingly popular for describing the photophysical properties of luminescent complexes, but to date, only a few studies of iridium(III) complexes have been reported.[3e,17a,b,18,31b,39,52b,63] Thus, absorption spectra were predicted by means of TD-DFT calculations based on S_0-optimized geometries (cf. the Supporting Information). The calculated absorption transitions reproduce well the principle spectral features and the energies (λ_{max}) of the absorption spectra for **9** as well as **8a**−**8g** (e.g., for **8a** and **8c**, parts A and C of Figure 10; see Figures S14−S29 in the Supporting Information for other complexes).

(54) (a) Becke, A. D. *J. Chem. Phys.* **1993**, *98*, 5648. (b) Becke, A. D. *Int. J. Quantum Chem.* **1994**, *S28*, 625. (c) Lee, C.; Yang, W.; Parr, R. G. *Phys. Rev. B* **1988**, *37*, 785. (d) Miehlich, B.; Savin, A.; Stoll, H.; Preuss, H. *Chem. Phys. Lett.* **1989**, *157*, 200.

(55) (a) Ditchfield, R.; Hehre, W. J.; Pople, J. A. *J. Chem. Phys.* **1971**, *54*, 724. (b) Hehre, W. J.; Ditchfield, R.; Pople, J. A. *J. Chem. Phys.* **1972**, *56*, 2257. (c) Hariharan, P. C.; Pople, J. A. *Theor. Chim. Acta* **1973**, *28*, 213. (d) Hariharan, P. C.; Pople, J. A. *Mol. Phys.* **1974**, *27*, 209. (e) Gordon, M. S. *Chem. Phys. Lett.* **1980**, *76*, 163.

(56) (a) Dunning, J. T. H. In *Methods of Electronic Structure Theory*; Schaefer, I., H. F., Ed.; Plenum Press: New York, 1977; Vol. *3*, p 1. (b) Hay, P. J.; Wadt, W. R. *J. Chem. Phys.* **1985**, *82*, 299. (c) Hay, P. J.; Wadt, W. R. *J. Chem. Phys.* **1985**, *82*, 270. (d) Hay, P. J.; Wadt, W. R. *J. Chem. Phys.* **1985**, *82*, 284.

(57) (a) Stevens, W. J.; Basch, W. J.; Krauss, M. *J. Chem. Phys.* **1984**, *81*, 6026. (b) Stevens, W. J.; Krauss, M.; Basch, H.; Jasien, P. G. *Can. J. Chem.* **1992**, *70*, 612. (c) Cundari, T. R.; Stevens, W. J. *J. Chem. Phys.* **1993**, *98*, 5555.

(58) (a) Schmidt, M. W.; Baldridge, K. K.; Boatz, J. A.; Elbert, S. T.; Gordon, M. S.; Jensen, J. H.; Koseki, S.; Matsunaga, N.; Nguyen, K. A.; Su, S.; Windus, T. L.; Dupuis, M.; Montgomery, J. A. *J. Comput. Chem.* **1993**, *14*, 1347. (b) Gordon, M. S.; Schmidt, M. W. In *Theory and Applications of Computational Chemistry: the First Forty Years*; Dykstra, C. E., Frenking, G., Kim, K. S., Scuseria, G. E., Eds.; Elsevier: Amsterdam, The Netherlands, 2005; p 1167.

(59) Bastiansen, O.; Samdal, S. *J. Mol. Struct.* **1985**, *128*, 115.

(60) Sancho-Garcia, J. C.; Cornil, J. *J. Chem. Theory Comput.* **2005**, *1*, 581.

(61) Johansson, M. P.; Olsen, J. *J. Chem. Theory Comput.* **2008**, *4*, 1460.

(62) Grumadas, A. J.; Poshkus, D. P.; Kiselev, A. V. *J. Chem. Soc., Faraday Trans. 2* **1982**, *78*, 2013.

(63) (a) Yang, C.-H.; Li, S.-W.; Chi, Y.; Cheng, Y.-M.; Yeh, Y.-S.; Chou, P.-T.; Lee, G.-H.; Wang, C.-H.; Shu, C.-F. *Inorg. Chem.* **2005**, *44*, 7770. (b) Polson, M.; Ravaglia, M.; Fracasso, S.; Garavelli, M.; Scandola, F. *Inorg. Chem.* **2005**, *44*, 1282. (c) Yang, C.-H.; Su, W.-L.; Fang, K.-H.; Wang, S.-P.; Sun, I. W. *Organometallics* **2006**, *25*, 4514. (d) Obara, S.; Itabashi, M.; Okuda, F.; Tamaki, S.; Tanabe, Y.; Ishii, Y.; Nozaki, K.; Haga, M.-a. *Inorg. Chem.* **2006**, *45*, 8907. (e) Liu, T.; Zhang, H.-X.; Zhou, X.; Zheng, Q.-C.; Xia, B.-H.; Pan, Q.-J. *J. Phys. Chem. A* **2008**, *112*, 8254.

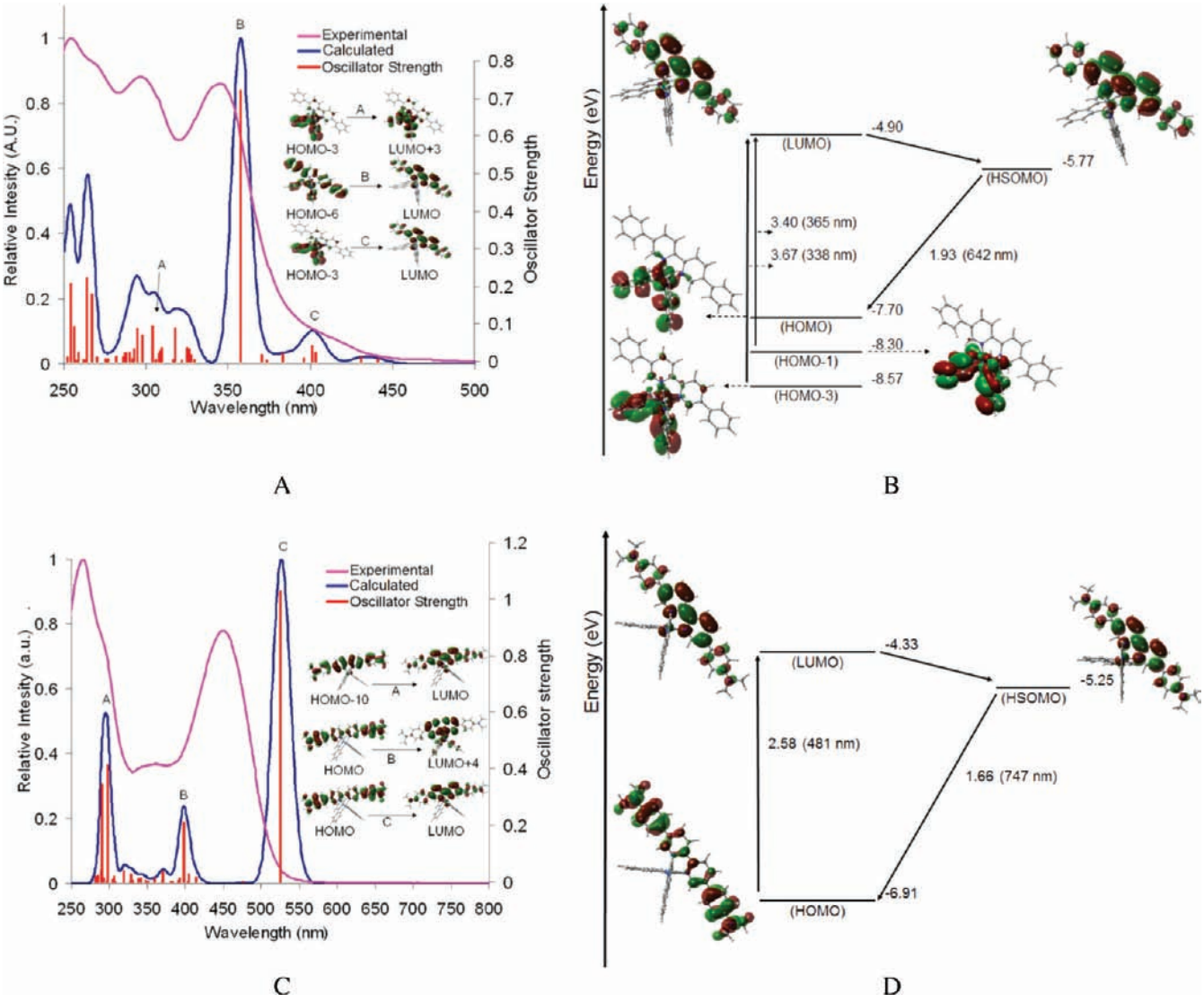

Figure 10. (A) Measured (violet) and simulated (blue) absorption spectra for **8a**. The oscillator strengths are represented by unbroadened vertical lines of calculated singlet−singlet transitions (red). (B) Calculated energies (for method 1, see the text) and isodensity surface plots for selected orbitals of **8a**. (C) Measured (violet) and simulated (blue) absorption spectra for **8c**. The oscillator strengths are represented by unbroadened vertical lines of calculated singlet−singlet transitions (red). (D) Calculated (for method 1, see the text) energies and isodensity surface plots for selected orbitals of **8c**.

The results indicate that, unlike **9**, **8a**−**8g** possess an additional and important allowed transition in the form of an ILCT that occurs on the ancillary ligand, wherein the arenes act as electron-releasing groups and the bpy ligand acts as the electron acceptor. The importance of this transition is evident in, for instance, **8c** and explains the dominant absorption band observed at ca. 450 nm (Figure 10C,D). What distinguishes series 1 (**8a**−**8c**) from series 2 (**8d**−**8g**) is that in the former this transition is dominant, in agreement with that observed in their absorption spectra. The lowest-energy permitted transition can be modulated by increasing the electron density of the arene. This has the effect of increasing the energy in both the π and π^* orbitals of the bpy* ligand, which correlates well with a free-energy relationship, as exhibited in Figure 11. Thus, whereas the lowest-lying permitted absorption transition with a significant oscillator strength is primarily comprised of a mixture of the π(ppy) → π^*(bpy*) transition (LLCT) with some MLCT character for **8a**, **8d**, **8g**, and **9**, the dominant low-energy absorption is that of an ILCT transition for the remainder of the complexes; **8g** also exhibits a low-energy transition with some $^1LC_{ppy}$ character (HOMO → LUMO+1). The orthogonal orientation of the aryl groups in **8d** and **8g** impedes electronic communication, effectively attenuating the intensity of the ILCT transition. Thus, the gross structure of their absorption spectra is essentially distilled to that of **9**. This is not the case for **8a**, where the aryl groups are somewhat implicated in the LUMO and the ILCT remains the dominant feature in the absorption spectrum. The first permitted transition for **8a** occurs for HOMO−1 → LUMO ($f \sim 0.01$). Additionally, there is a second important transition, HOMO−3 → LUMO ($f \sim 0.04$), wherein the occupied MO is nearly isosymmetric with the first and that of the HOMO ($f \sim 0.0004$ for HOMO → LUMO) (cf. Figure 10B). Complex **8d** behaves similarly, with the first permitted transition occurring for HOMO−1 → LUMO ($f \sim 0.01$), with the presence of a second important transition, HOMO−3 → LUMO ($f \sim 0.03$). For **8g**, absorption occurs primarily from a mixed

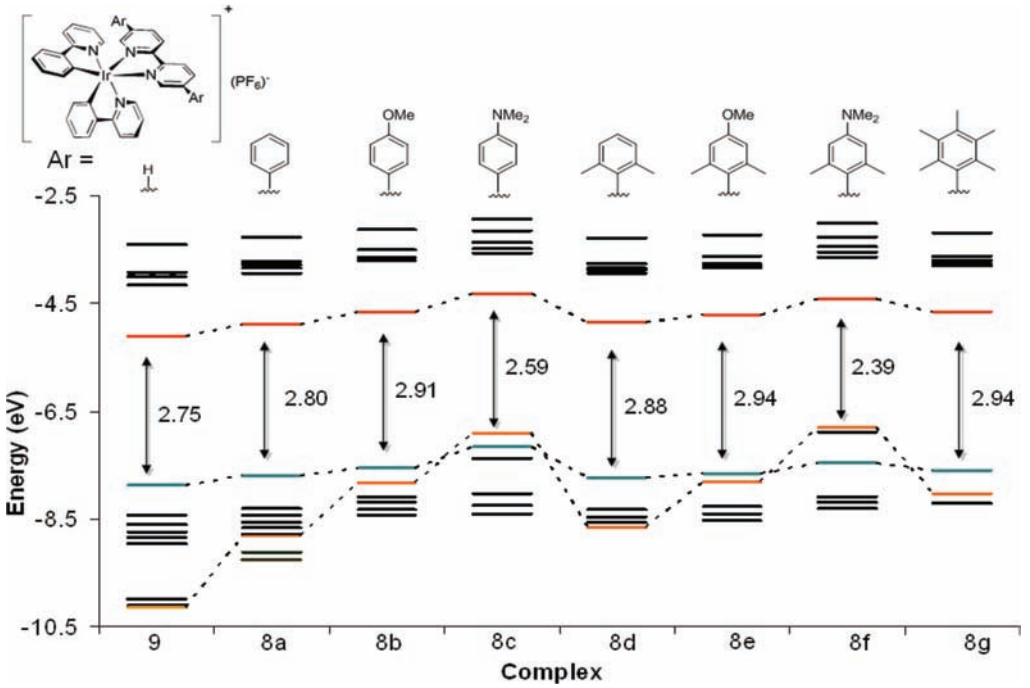

Figure 11. Calculated electronic structures for **9** and **8a**−**8g** by DFT methods at their S_0-optimized geometries (see the text). Black indicates that the electron density is mostly localized on π(bpy) and π(ppy) with contributions from d(Ir). Orange and turquoise indicate the most energetic π(bpy) and π(ppy), respectively. In each of these cases, minor d(Ir) contributions may exist. Red indicates the LUMO, which is localized on π^*(bpy).

HOMO → LUMO+1 and HOMO → LUMO+2 transition (f = 0.027; 74:21), which is characterized as an admixture of ^{1}LC and ^{1}LLCT. There is an additional important ^{1}LLCT/^{1}MLCT transition, HOMO−7 → LUMO ($f \sim$ 0.04), which is close in energy to the first (see Figure S20 in the Supporting Information).

Although DFT/TD-DFT calculations predict the general form of the absorption spectra for **8b** and **8c** and for **8e**, and **8f**, they poorly estimate absorption energies; the predictions are bathochromically shifted by ca. 70 and 150 nm for **8b** and **8c** and for **8e** and **8f**, respectively (cf. Figures S22−S29 in the Supporting Information). The bathochromic shift for **8b** and **8c** (e.g., Figure 10C for **8c**) can be rationalized by the difference in conformation between the gas-phase and solution-state structures existing at RT. More likely is that there is an overestimation of the planarization computed in the triplet state. For each of these four complexes, the transition from the ground state to the lowest-energy singlet (S_1) state [HOMO−1→LUMO for **8b** ($f \sim 0.57$) and **8e** ($f \sim 0.09$); HOMO → LUMO for **8c** ($f \sim 1.03$) and **8f** ($f \sim 0.43$)] involves primarily a π(bpy*)−π^*(bpy*) ^{1}ILCT transition. The oscillator strength for this transition is particularly large ($f > 0.6$) for **8b** and **8c** but hypochromically shifted by over 60% for **8e** and **8f** because of the orthogonal orientation of the aryl groups in these complexes, a characteristic also observed experimentally. Complexes **8b** and **8e** also exhibit a low-energy admixture of LLCT and MLCT transitions (HOMO−4 → LUMO for **8b**; HOMO−5 → LUMO for **8e**), similar to those described for the other complexes in this study. In the particular case of **8e**, this transition is, in fact, more dominant than the lower-energy ^{1}ILCT transition. The absence of evidence for this contribution to low-energy transitions for **8c** and **8f** is a result of the increased electron density contribution of the NMe_2 groups incorporated onto each, which has the effect of raising both the HOMO and LUMO energy levels. In fact, the next-lowest-lying transition after the characteristic ILCT transition was identified as ^{1}LMCT.

Table 7. Comparison of Experimental and Calculated Emission Energies for **9** and **8a**−**8g**

	experimental emission (nm)		calculated emission (nm)			
complex	77 K[a]	298 K[a]	method 1[b]	method 2[c]	relative error (%)[d]	method 3[e]
9	532	595	549	561	5.5	619
8a	531	623	642	551	3.7	592
8b	551	613	690	576	4.5	566
8c	619	659	747	659	6.5	669
8d	516	599	563	541	4.8	580
8e	506	596	608	564	11.4	567
8f	563	613	735	633	12.3	676
8g	513	592	570	530	3.3	566

[a] λ_{max}. [b] $\Delta E = E^{T_1}_{HSOMO} - E^{S_0}_{HOMO}$. [c] $\Delta E = E^{T_1}_{total} - E^{S_0}_{total}$. [d] Calculated between method 2 and experimental emission at 77 K. [e] $\Delta E = E^{T_1}_{total} - E^{S_0}_{total}$ by TD-DFT.

Emission energies were calculated using three distinct methods found in the literature. For the first two methods, we imposed a triplet spin multiplicity by selectively populating the LUMO on complexes whose geometries had been previously optimized at the S_0 state. The geometry of the newly formed HSOMO triplet (T_1) state was then reoptimized at the same level of theory (using UB3LYP) to account for any geometry relaxation in the triplet excited state. Method 1[17b,31a,64] calculates the energy difference between HSOMO(T_1) and HOMO(S_0), while method 2[3g] calculates the energy difference between

(64) Brooks, J.; Babayan, Y.; Lamansky, S.; Djurovich, P. I.; Tsyba, I.; Bau, R.; Thompson, M. E. *Inorg. Chem.* **2002**, *41*, 3055.

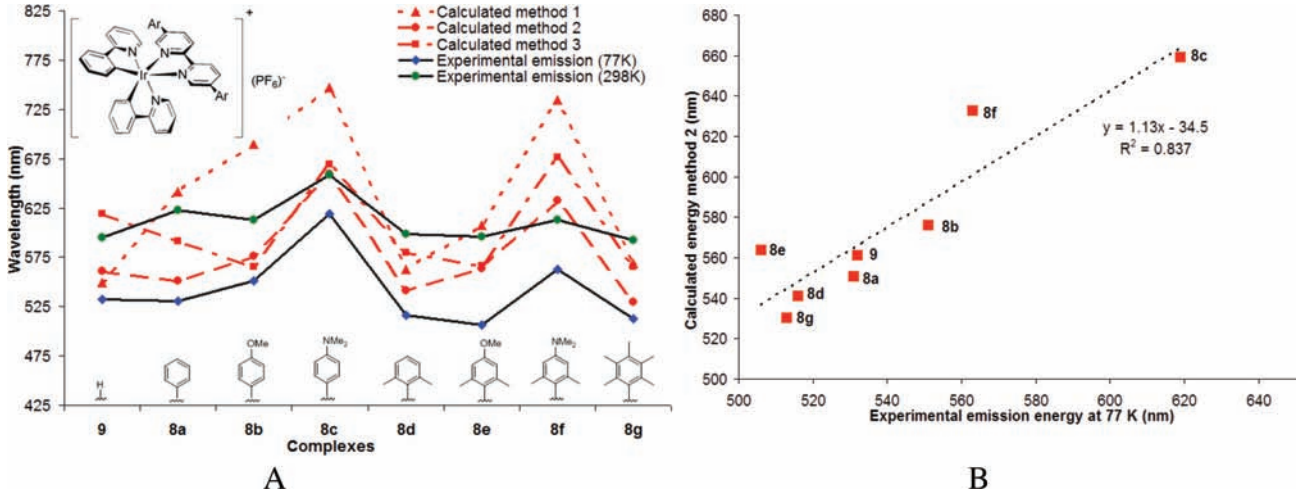

Figure 12. (A) Comparison between experimental (77 and 298 K) and calculated emission energies (λ_{max}) using methods 1−3 for **8a**−**8g** (see the text). (B) Comparison between calculated (method 2) and experimental emission energies at 77 K (λ_{max}).

the T_1 and S_0 states (ΔSCF approach). Method 3 calculates the energy difference between the T_1 and S_0 states as determined directly from TD-DFT methods using restricted B3LYP.[65] The calculated emission energies using these three methods are summarized in Table 7, and a comparison with those measured is shown in Figure 12.

The electronic structures, as illustrated by the orbital patterns, in the T_1 state are similar to those found for the S_1 state (e.g., Figures 10B,D and S14−S21 in the Supporting Information). The electronic structures obtained from DFT calculations indicate that emission (HOMO ← LUMO) for all complexes, except **8c** and **8f**, can be described as mainly an admixture of LLCT/MLCT transitions. In these latter two cases, emission is best described as occurring through an ILCT transition. The predicted emission energies not surprisingly better reflect those measured at 77 K because at this temperature the frozen conformation is better mirrored to that of the predicted geometry. Overall, all three methods systematically underestimate the emission energy;[66] however, method 2 correlates quite accurately with experiment, as demonstrated by the overall linear fit found in Figure 12B. Charge-density analysis for **8d**−**8g** indicates that functionalization at the 4′ position has essentially no impact up the electronics of the bpy ligand, and thus there is negligible electronic communication through the σ network. These results suggest that the aryl groups in **8d**,**8e**, and **8g** essentially act to shield the iridium center without affecting much the luminescence properties of the complexes.

Conclusion

We have synthesized, studied computationally, and measured the photophysical and electrochemical properties of a series of new cationic iridium(III) complexes based on 5,5′-diaryl-2,2′-bipyridines as ancillary ligands. These combined studies indicate that intense emission in ACN occurs primarily from a mixed ^{3}MLCT and ^{3}LLCT transition except for those complexes bearing dimethylamino substituents at the 4′ position of the aryl groups. These latter complexes emit with much diminished intensity from a ^{3}ILCT state. Modest emission wavelength tuning of (ca. 30 nm) at RT was achieve by increasing the effective conjugative length of the ancillary ligand. Complexes with aryl substituents bearing *o*,*o*-dimethyl groups do not impact the emission energy at RT because of their relative orthogonal orientation with respect to the bpy plane, yet they emit brightly in the orange, with quantum yields ranging from 16 to 22% in ACN, except for **8f**. The appending of peripheral aryl groups about the bpy ancillary ligand to promote supramolecular π-stacking interactions has recently been shown to increase the device stability.[67] The use of ancillary ligands such as ours, which can effectively shield the iridium(III) center and its bonding to the surrounding ligands from adventitious attack by small molecules, would be amenable to exploiting this same interaction.[3d] In fact, with the exception of **8c** and **8f**, the complexes within this study luminesce in the orange-red as brightly as the best cationic iridium-based luminophores found in the literature. The construction and physical and photophysical characterization of LEECs using our complexes will be reported elsewhere.

Our calculations demonstrate that method 2 is the most accurate for reproducing experimental emission energies. The TD-DFT study provides insight into the origin of the transitions. Combined DFT/TD-DFT calculations indicate that frequently the S_0-state HOMO orbitals are localized over the ppy cyclometalating ligand and the iridium center, whereas the LUMO is mainly localized on the bpy fragment.

Acknowledgment. We acknowledge Professor Pierre D. Harvey for helpful discussions and for access to the fluorimeter and UV spectrophotometer found in his laboratory. We thank M. Shawkat Aly for aide during fluorimetry measurement acquisition. We thank Professor Christian Reber for modeling the low-temperature emission spectra.

(65) The primary difference between methods 1 and 3 is the following. For method 1, the energies of the S_0 and T_1 states are computed separately to obtain optimized MOs for each of these states, with the latter defined as an $m_l = 1$ state. In the case of method 3 (using TD-DFT), the excited states are expanded as determinants built from the ground-state (S_0) orbitals and the triplets are formally assigned an $m_l = 0$ state and are coupled as two determinants: single excitation HOMO/LUMO α with HOMO/LUMO β with a positive sign.

(66) (a) Grimme, S.; Parac, M. *ChemPhysChem* **2003**, *4*, 292. (b) Jacquemin, D.; Perpete, E. A.; Scuseria, G. E.; Ciofini, I.; Adamo, C. *J. Chem. Theory Comput.* **2008**, *4*, 123.

(67) Graber, S.; Doyle, K.; Neuburger, M.; Housecroft, C. E.; Constable, E. C.; Costa, R. n. D.; Ortiz, E.; Repetto, D.; Bolink, H. J. *J. Am. Chem. Soc.* **2008**, *130*, 14944.

We also acknowledge Professor Jean Lessard for access to CV instrumentation and Dr. Jean Marc Chapuzet for aide in voltammogram interpretation. Computational time on the Mammouth supercomputer at the Université de Sherbrooke was underwritten by RQCHP (réseau québécois de calculs de haute performance). E.Z.-C. acknowledges CFI (Canadian Foundation for Innovation), NSERC (the National Sciences and Engineering Research Council of Canada), FQRNT (Le Fonds québécois de la recherche sur la nature et les technologies), and the Université de Sherbrooke for financial support.

Supporting Information Available: X-ray crystallographic data for **8a** and **8g** in CIF format, complete experimental procedures for all new compounds, methodologies used for photophysical and electrochemical characterization, details of computational methodology, ^{1}H NMR comparison of the chloride and PF_6 salts for **8d**, calculated low-temperature emission spectra, cyclic voltammograms for **8a**−**8g** and **9**, table of calculated S_1 and T_1 geometries for all complexes, table of population analysis for four HOMOs and four LUMOs for all complexes, calculated absorption and emission energies and isodensity surface plots for selected orbitals of **8a**−**8g**, tables of the 50 lowest-energy transitions calculated by TD-DFT for **8a**−**8g** and **9**, simulated (red) absorption spectra for **8a**−**8g** [the oscillator strengths are represented by unbroadened vertical lines of calculated singlet−singlet transitions (green)]. This material is available free of charge via the Internet at http://pubs.acs.org.